═══ *Hetero- and low-dimensional structures* ═══

Luminescent properties of the structures with embedded silicon nanoclusters: Influence of technology, doping and annealing (Review)

V.P. Melnik, V.G. Popov, B.M. Romanyuk, S.V. Antonin[*], A.A. Evtukh

V. Lashkaryov Institute of Semiconductor Physics, NAS of Ukraine
41, prosp. Nauky, 03680 Kyiv, Ukraine
[*]*Corresponding author e-mail: antoninsv@gmail.com*

Abstract. Detection of photoluminescence (PL) in traditionally non-luminescent Si material (a typical indirect band semiconductor) attracts great attention both in the scientific aspect and for applications in the field of micro- and nanoelectronics and photoelectronics. Despite the success in technology and understanding of many features inherent to its PL characteristics, many problems have not yet been resolved. In particular – what is the origin of PL lines: quantum size, molecular complexes within SiO_2, interface or volume localized states, *etc*. How to achieve the increase in the PL intensity and to provide excitation of it in different parts of the spectrum. The proposed review systematizes results of studies associated with these problems concerning the original technologies for creation of Si nanocrystals (nc-Si) and various research methods. In conclusion, we summarize the results on the properties of nc-Si-SiO_2 luminescent structures depending on their technology of synthesis, photo- and structural features and application prospects for micro- and nanoelectronics as well as photoelectronics.

Keywords: silicon, nanocluster, photoluminescence, ion-beam synthesis, doping, annealing.

1. Introduction

Interest to the structures with nanoclusters is caused by the unique properties inherent to these structures, which can be radically different from the properties of bulk material. For the recent decades, the photoluminescence (PL) properties of the silicon nanocrystals and systems containing them are under intensive investigations due to the prospects for creation of Si-based optoelectronic devices [1–6]. Potential applications are sensing, photovoltaics, LED color converters, medical imaging, *etc*. The origin of PL in systems containing nc-Si is related to either the quantum confinement effect or recombination through the surface states. In many cases of Si-based nanostructures, both mechanisms play an important role.

Structures with nanoscale silicon crystalline inclusions embedded into the dielectric film, usually the amorphous film of silicon dioxide, are of great interest. These silicon nanoclusters (Si-nc) are capable of emitting light in the visible and near-IR regions of the spectrum, accumulate and storage of the electric charge. This opens up prospects for their wide practical application: creation of cheap light-emitting elements in which the wavelength of emitted light can be controlled, formation of memory cells and development of a new generation of sensor systems sensitive to different types of radiation. Since silicon technology is and will remain the basis of modern micro/nanoelectronics in the nearest future, these structures can be easily integrated into the technological process. In particular, they can become local sources or sensors of radiation in chips, which will solve some problems of electrical connections. To do this, in structures based on Si-nc it is necessary to increase the intensity of radiation, to ensure the stability and control of the radiation spectrum.

Solving these problems requires understanding the physical mechanisms and study of the processes that occur during operation of such systems under the influence of external factors, improving methods of their creation to ensure reliability and expand possible applications.

In this review, the influence of the number of factors (presence of impurities, deposition method, composition of SiO_x film and annealing temperature) on formation and luminescent properties of the structures based on Si-nc have been considered, as well as the influence of some external factors (ionic doping and low temperature treatments) on modification of $Si-nc/SiO_2$ interfaces have been studied. Physical mechanisms that explain the influence of these factors on the luminescence of these structures have been analyzed.

2. Methods of ion-beam synthesis and modification of silicon luminescent structures

2.1. Synthesis of structures with Si-nc embedded into SiO₂

Many methods have been proposed for the synthesis of structures with silicon nanoclusters embedded into the dielectric matrix, most of which are based on the decay of the nonstoichiometric SiO_x film ($x < 2$) during high-temperature annealing. For the formation of nonstoichiometric SiO_x films ($x < 2$), plasma chemical deposition from the gas phase (plasma-enhanced chemical vapor deposition – PECVD) [7–13], chemical deposition from the gas phase at low pressure vapor deposition – LPCVD) [14–17], silicon target sputtering with the electron gun [18] or ion plasma [19, 20] in the controlled oxygen atmosphere, pulsed laser sputtering in an inert atmosphere [21], thermal evaporation of SiO (or SiO_y) powder [22, 23], ion implantation in various modes [13, 24–28], *etc.* are used (see Fig. 1). Most of these methods allow to change the silicon content in the film in the controlled way depending on the technological parameters of the SiO_x film synthesis process.
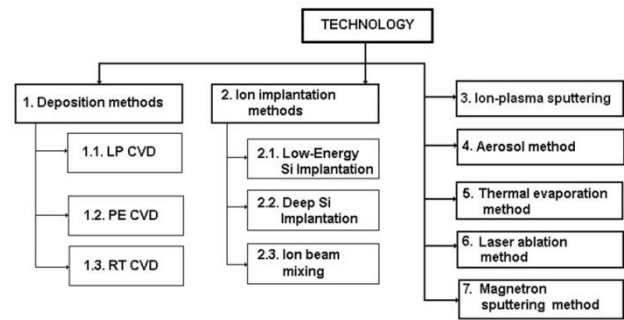

Fig. 1. Technologies of Si rich SiO_x films and Si-nc formation.

2.2. Growth and structural properties of Si-nc in SiO₂

Si nanoclusters in SiO_2 matrix are formed in the process of diffusion-controlled decay of the SiO_x phase at silicon concentrations higher than $10^{21}\,cm^{-3}$ (degree of super-saturation ~ 1 at.% and more) and annealing temperatures above 900 °C. In the SiO_x film at high concentrations of excess silicon, the latter likely forms complexes and small inclusions of silicon chain or fractal type even without annealing, which are detected using the Raman spectra and X-ray photoelectron spectroscopy (XPS). They act as seeds in formation of silicon phase [29]. In the diffusion process of the Si inclusions formation under phase transformation of nonstoichiometric SiO_x films there are two stages. At the first stage, fluctuations promote formation of new phase seeds and their growth directly from the supersaturated solution. At the second stage, the Oswald process of "maturation" plays a decisive role, which consists in dissolving nanoclusters with a size smaller than the critical one, and respective growth of large Si-nc. This process is caused by minimization of free energy of the system, in particular, minimization of the interfaces between the phases. In the limiting case, one single crystal should be formed in the surrounding matrix of stoichiometric SiO_2 [30]. In [31] it was shown that the experimentally determined values of the diffusion coefficient at diffusion-limited growth of Si-nc differ significantly from the diffusion coefficient of silicon in SiO_2 and are close in value to the oxygen diffusion coefficient. According to the authors, the basis of thermostimulated phase separation of SiO_x is the mobility of oxygen atoms, which is consistent with the data of [32].

Experimental data and theoretical modeling indicate the presence of the transition layer with the thickness of 8…10 Å between the Si-nc and the SiO_2 matrix [33–35]. This transition layer is mechanically stressed [36], while mechanical stresses in the matrix outside this layer are absent [35].

In the case of deposited silicon suboxide film, a homogeneous distribution of nanoclusters over the film volume is usually obtained. In the case of ion implantation, the concentration of Si-nc and their average size are maximal at the depth of the design run of ions.

Melnik V.P., Popov V.G., Romanyuk B.M. et al. Luminescent properties of the structures with embedded silicon …

279

Transmission electron microscopy (TEM) is the most effective method for analyzing the distribution of nanoclusters in the volume, determining their size and shape. Statistical analysis of the images obtained using TEM shows that with increasing the annealing temperature of the SiO$_x$ film, the average diameter of the nanocluster increases [37, 38]. Similarly, the increase in the concentration of silicon in the film leads to the increase in the average size of Si-nc at a given annealing temperature [39]. In [40] attention was paid to the fact that the dimensions of Si-nc can acquire only discrete values: $d = d_0 + 2na$, where $a = 0.314$ nm – lattice constant, $n = 0, 1, 2, …$ It should be noted that the bond length Si-Si in Si-nc differs from the value characteristic for bulk silicon [41], so the values of the "allowable" sizes of Si-nc may differ slightly from those described in [40].

2.3. Luminescence of structures with Si-nc

The difference between the luminescent properties of Si-nc and the properties of bulk silicon is due to the quantum-size effect. For excitons (or electron-hole pairs), the silicon nanocluster embedded in the dielectric matrix is the potential spherical well with the high potential barrier (3.2 eV for electrons and 4.3 eV for holes [42]) due to the presence of the dielectric matrix. Quantum-size effect is observed in nanoclusters, the average size of which does not exceed the value of the Bohr radius for the exciton in this semiconductor is $a_b = \dfrac{4\pi h \varepsilon \varepsilon_0}{\mu e^2}$, where h is the Planck constant, ε is the relative dielectric constant of this semiconductor, ε_0 is the electric constant of vacuum, e is the electron charge $\mu = \dfrac{m_e m_h}{m_e + m_h}$ is the reduced mass of the electron-hole system, m_e, m_h are the effective masses of electron and hole, respectively. For silicon, the Bohr radius is $\sim a_b(\text{Si}) = 4.3$ nm, so the effect of quantum localization is observed for structures with silicon nanoclusters, the size of which does not exceed 4.3 nm. In the case of the infinite potential barrier at the Si-nc/SiO$_2$ interface, the band gap for the nanocluster can be determined using the formula given in [43]:

$$E_g^{nc} = E_g^{\text{Si}} + \frac{h^2}{8m_e^* L^2} + \frac{h^2}{8m_h^* L^2}, \qquad (1)$$

where E_g^{Si} is the band gap of silicon, L is the nanocluster size, m_e^* and m_h^* are the effective masses of electron and hole, respectively. In [44], the procedure for calculating the band gap of spherical Si-nc from its diameter is described in detail, considering the limited potential barrier at the Si-nc/SiO$_2$ boundary.

Thus, since the size of the nanocluster decreases, the energy associated with recombination of exciton (or electron-hole pair) increases, the wavelength of the emitted light should decrease. In addition, the quantum-size effect increases the probability of radiative recombination of electron-hole pairs (and/or excitons) localized in the nanocluster. Spatial quantum-size localization of the electron-hole pairs in the nanocluster "simplifies" the conditions for fulfilling the law of conservation of the momentum during radiative recombination.

As a rule, three characteristic regions are separated when analyzing the PL spectra, namely: (1) blue-ultraviolet region ($\lambda = 280…480$ nm), (2) yellow-green region ($\lambda = 490…590$ nm) and (3) red region ($\lambda = 620…950$ nm). Our analysis of the first PL region is mainly based on the qualitative consideration of the influence of preparation technology and the following treatments [45, 46]. It was concluded that PL in this range is not caused by the quantum-size effect but by radiative transitions between energy levels of oxygen vacancies in silicon oxide matrix [47]. Yellow-green PL band usually has low intensity and origins from radiative recombination in nanoparticles and stressed Si crystals. Finally, red PL band is caused by recombination processes in silicon quantum dots (Si-QD) [48, 49]. The structure of Si-QD significantly influences on the position of red PL band. Amorphous Si nanoinclusions emit quanta of higher energies in comparison with those in crystals [50, 51]. There is also another separation of PL spectra based on the conception of two dominant bands: the "Slow" (S) band in the red-yellow spectral range with long microsecond decay times and the "Fast" (F) band in the blue-green range with faster nanosecond decay times [1].

The influence of the temperature on the luminescence spectrum [7, 52, 53], size of nanoclusters and their size distribution [39, 54], temperature and duration of annealing [7, 10, 39, 55], and for structures obtained by ion implantation, dose of implanted ions [55, 56] and the temperature of the samples during implantation [57, 58] are described in the literature in detail.

The maximum intensity of PL was observed at different concentrations of excess silicon in the film: from ~10 at.% to ~30 at.% [38]. The optimum annealing temperature of SiO$_x$ films at which the maximum PL is observed depends on the concentration of silicon, but is usually within the range of 1100 to 1150 °C [7, 38]. In this case, increasing the annealing temperature leads to the shift of the maximum PL to the long-wave region [7].

The position of the PL band does not change with increasing annealing time for more than 1 hour, since the whole "population" of nanoclusters is formed during the first annealing hour [59]. Increasing the PL intensity with the annealing time of 2 to 4 hours is associated with passivation of nonradiative P_b centers by oxygen [37, 38].

2.4. Modification of light-emitting structures with Si-nc

For practical use, an important task is to increase the PL intensity of these structures, so there observed is an intensive search for ways to increase its efficiency.

Melnik V.P., Popov V.G., Romanyuk B.M. et al. Luminescent properties of the structures with embedded silicon …

280

In general, methods for modifying structures with Si-nc can be separated into two groups: (*i*) methods associated with the implantation of impurities and (*ii*) methods associated with heat treatment of these structures. Often this modification includes the combination of these two methods. Methods of combined modifications, such as the effect of γ-irradiation followed by heat treatment [60], should be singled out.

Modification of structures with Si-nc due to implantation of the impurities. Doping impurities can affect the process of formation of Si-nc (C, Au, Al, Ti), defective and electronic structure of the material (P, B, H), can change the probability of radiative and nonradiative transitions (H, N, O), can change the mechanism of radiative recombination in these structures (Er, Yb, Tm, Tb).

To increase the intensity of PL structures with Si-nc use hydrogen doping, which is carried out by annealing (~ 500 °C) in an atmosphere of "forming gas" (a mixture of hydrogen and nitrogen or argon) [61, 62] or implantation of hydrogen ions followed by thermal annealing [63]. Most of authors associates this significant increase in PL intensity with the passivation of H broken bonds, which are the centers of nonradiative recombination.

Nitrogen admixture attracts special attention of researchers because the nitrogen is one of the main components of the gaseous medium (N_2O) during gas-phase deposition of SiO_x films and can be introduced into Si-nc structures during annealing in N_2 atmosphere [8, 64] or implanted in the form of N_2^+ during the implantation of silicon as the uncontrolled impurity. The presence of a sufficiently high concentration of nitrogen (1…10 at.%) changes the structure of the matrix (oxynitride matrix SiN_xO_y), which surrounds Si-nc [64]. The presence of nitrogen slows down the diffusion of silicon and prevents formation of Si-nc [65, 66]. On the other hand, Si-N bonds can also be additional centers of silicon precipitation in SiO_x films at a certain ratio of nitrogen and excess silicon concentrations in the film [67]. This leads to the increase in the concentration of nanoclusters and the intensity of PL.

Carbon doping of SiO_x original films or structures with formed Si-nc leads to PL bands with maxima around 400, 500 nm, which are associated with formation of SiC and C nanoclusters [68] or with the defects [69]. The effect of C on the properties of Si-nc structures based on porous silicon was studied in [70], in which the occurrence of the PL band with the maximum of about 500 nm was associated with the formation of carbon inclusions.

The presence of Al in SiO_x films during thermal decomposition stimulates the formation of defects that are the centers of luminescence and causes long-wave shift of the PL band [71]. The interaction of Al with O stimulates the formation of oxygen vacancies, with which the authors associate the PL band in the region of 820 nm.

Modification of structures with Si-nc due to thermal treatment. The properties of the structures with formed Si-nc [65, 72] or synthesized SiO_x films before forming annealing can be modified by heat treatments [73, 74].

To increase the concentration of Si-nc nuclei, the synthesized SiO_x films were subjected to rapid thermal annealing [74] or performed conventional annealing at temperatures of 500…800 °C [73]. Such treatment stimulated the nucleation of nanoclusters and led to an increase in the intensity of PL of the structures formed on the basis of such modified silicon suboxide.

Another way to modify the structure with Si-nc is to carry out heat treatments after the formation of the structure. One of these treatments is passivation in the H_2 atmosphere. Similarly, annealing of structures with formed Si-nc in the atmosphere of O_2 ($T_a = 500$ °C) leads to a significant increase in PL, which is associated with passivation of broken bonds by O at the interface Si–nc/SiO_2 and oxidation of Si-nc. Higher stability of Si–O bonds, as compared to Si–H, is considered to be a significant advantage of this treatment.

Despite intensive research, there is still no consensus on the mechanisms of radiative recombination in the structures with Si-nc, and the results of studying the light-emitting properties of these structures often contradict each other. Confirmation of the reliability of the mechanism is important for understanding the fundamental features of nanoscale systems. For further practical use of the structures with Si-nc, it is important to increase the intensity and expand the spectral range of radiation, which can be realized by ion-beam synthesis and modification of these structures.

3. Synthesis and diagnostics of structures with silicon nanoclusters embedded into the dielectric matrix

To clarify the specifics of formation processes for the structures with silicon nanoclusters depending on the method for synthesizing the initial SiO_x ($x < 2$) films, three methods, namely, plasma-enhanced chemical deposition from the gas phase, thermal evaporation and ion implantation have been used by the authors.

3.1. Preparation of SiO_x suboxide films

Plasma-enhanced chemical vapor deposition (PECVD). SiH_4 and N_2O gases were used as the precursors. Changing the flow ratio of reagent gases enables to change the concentration of the excess Si in the deposited film. This method allowed to synthesize the nonstoichiometric silicon oxide films with the thickness from several tens of nanometers up to several hundreds.

Thermal evaporation of SiO powder in vacuum. The powder is heated in the holder to the temperatures between 1000 and 1200 °C in the vacuum chamber. SiO_x film is deposited onto the substrate, and its composition is defined by the substrate temperatures, the type of source, the pressure in the working chamber and the deposition rate (see [75] for more details).

Melnik V.P., Popov V.G., Romanyuk B.M. et al. Luminescent properties of the structures with embedded silicon …

281

Ion implantation. Silicon ions with the energies from 30 up to 150 keV were implanted into silicon oxide films [76, 77]. Since the ion current density during implantation is low (0.3…2 µA/cm^2), implantation does not lead to significant heating of the substrate (1…10 °C). To analyze the effect of substrate temperature on the properties of synthesized structures "hot implantation" (the film in which the ions were implanted was heated to the temperature of ~ 450 °C) was performed. Due to the temperature dependence of the recombination of radiation defects formed in the film during implantation, the ability to control the substrate temperature allows to change the structure of synthesized samples.

The use of ion implantation to create nano-objects requires large doses of implanted ions and is accompanied by generation of the large number of radiation defects, which largely define the properties of the synthesized structures. That is, having the ability to control the change in the structure of radiation defects, one can effectively control the properties of nanostructures.

To control the system of radiation defects, the ultrasonic treatment of the substrate during the ion implantation process – acoustically stimulated ion-beam synthesis – also have been used [77–79]. According to the results of secondary ion mass-spectroscopy (SIMS) measurements, the ultrasonic treatment of the substrate during the process of silicon ions implantation of the SiO$_2$ film changes the thickness distribution profile of the silicon in the film. Fig. 2 shows the experimentally obtained distribution profile of silicon in the sample implanted with the ultrasonic treatment (f = 9.5 MHz, P = 1 W/cm^2). The presence of an ultrasonic wave in the substrate changes the spatial distribution of the radiation defects [78, 79], which, in turn, leads to the change in the distribution of implanted silicon.

SiO$_x$ films synthesized by ion implantation, in comparison with deposited films have several significant features:

1) the distribution of silicon over the film thickness is heterogeneous and is defined by the energy of implantation;

2) there is the area with the maximum concentration of silicon, and its position (depth in the sample) can be controlled (by changing the energy of implanted ions);

3) the concentration of silicon in the film can be changed precisely by changing the dose of implanted ions;

4) the deviation of the elemental composition of the film from that provided by theoretical calculations at given process parameters is insignificant. Assuming the concentration of Si atoms in SiO$_2$ equal to $n_{Si}(SiO_2)$ = 2.2·10^{22} atoms/cm^3 and the concentration of oxygen atoms – $n_O(SiO_2)$ = 4.4·10^{22} atoms/cm^3 [32, 80] and, calculating the distribution of implanted ions along the depth of the film, one can determine the concentration of Si at any depth of the film by using the following formula:
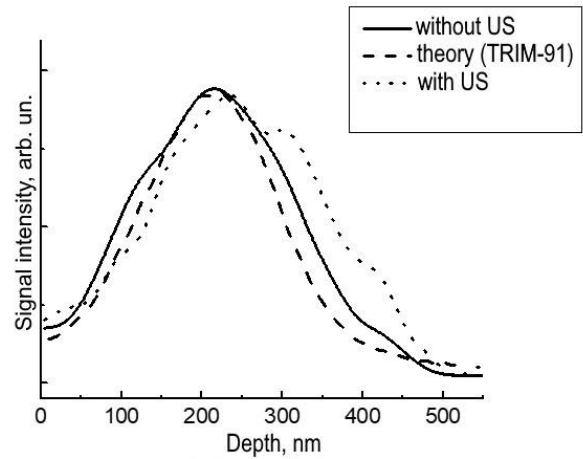
Fig. 2. The distribution profile of the silicon along the depth of the SiO$_2$ film (d = 600 nm) implanted with ^{28}Si$^+$ ions with an energy of 100 keV and a dose of 6·10^1 ions/cm^2.

$$C_{Si} = \frac{n_{Si}(SiO_2) + n_{Si}^{impl}}{n_{Si}(SiO_2) + n_O(SiO_2) + n_{Si}^{impl}} \cdot 100\% , \qquad (2)$$

where n_{Si}^{impl} is the concentration of implanted ^{28}Si$^+$ ions at the given depth.

The elemental composition of SiO$_x$ films was determined using X-ray photoelectron spectroscopy (XPS) and Auger electron spectroscopy, and the depth distribution of the elements was evaluated by SIMS. The composition of SiO$_x$ films prepared using plasma chemical deposition, and thermal evaporation was almost uniform in the sample. The content of silicon in the studied films varied in the controlled manner from 35 to 40%, in addition to silicon and oxygen, the small amount of nitrogen (< 1%) and carbon (~ 2%) was detected in the films.

3.2. Thermal decomposition of SiO$_x$ phase and formation of Si-nc

Since the state of the Si-O system in the form of suboxide is metastable, the process of suboxide decomposition into Si and SiO$_2$ with increasing temperature is observed. The process of diffusion decay of the SiO$_x$ phase can occur in two different ways: i) nucleation of silicon clusters, their diffusion growth and Oswald's "maturation"; ii) spinodal decay, surface minimization and Oswald's "maturation". The way in which the SiO$_x$ phase will decompose depends on the concentration of silicon in the film: at low concentrations, the first process is more probable, at high concentrations, the second one is realized [81]. Since in the films under studying, the concentration of excess silicon did not exceed 10 at.%, the phase decay in this case, most likely, occurred in the first scenario: nucleation → diffusion growth → Oswald's "maturation".

*Melnik V.P., Popov V.G., Romanyuk B.M. et al. Luminescent properties of the structures with embedded silicon …*

282
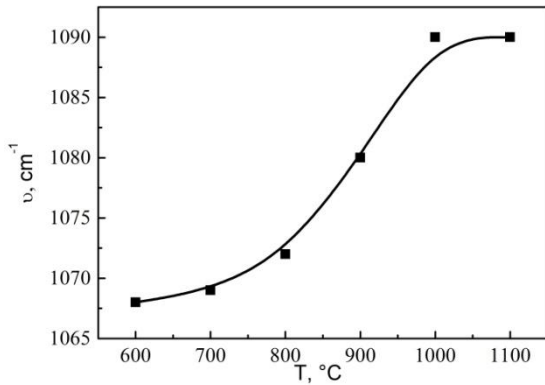
Fig. 3. Dependence of the position of IR absorption band maximum on the annealing temperature for thermally evaporated $SiO_{1.5}$ film ($d = 250$ nm).

Fig. 4. AFM image of the film surface with Si-nc obtained using ion implantation.

The process of diffusion decay of the SiO_x phase at high temperatures (> 1000 °C) leads to formation of silicon nanocrystals surrounded by the dielectric matrix, the composition of which corresponds almost to silicon dioxide [31]. The process of phase separation in the SiO_x film after annealing at lower temperatures is associated with formation of silicon inclusions in the SiO_y matrix ($x < y \leq 2$), the composition of which differs from SiO_2 [82].

Changing the composition of the surrounding matrix from SiO_x to SiO_y ($x < y \leq 2$) shifts the position of the IR absorption band maximum to characteristic for Si–O bonds (about $1000...1080$ cm^{-1}) [72]. Moreover, with increasing stoichiometry index (y) the position of the band is shifted toward increasing the wavenumber: for $y = 1$, position of the maximum close to 1000 cm^{-1} [22], and for $y = 2$ it is about $1075...1093$ cm^{-1} [83]. As can be seen in Fig. 3, the IR absorption band maximum is shifted in the direction of the wavenumber with increasing the annealing temperature and at annealing temperatures of $1000...1100$ °C, the maximum position corresponds to the value typical for SiO_2. This shift is associated with the increase in the stoichiometry index (y) of the surrounding SiO_y matrix from x to 2, with increasing annealing temperature [84, 85].

Confirmation of the formation of silicon nanoclusters after high-temperature annealing was obtained by using atomic force microscopy (AFM) and transmission electron microscopy (TEM).

Fig. 4 shows images of the surface of silicon oxide film with embedded Si-nc obtained using AFM. The test sample was prepared by implanting Si$^+$ ($E = 100$ keV, $D = 6 \cdot 10^{16}$ cm^{-2}) into the film of SiO_2 ($d = 600$ nm), followed by high-temperature annealing at 1100 °C for 20 min in the inert atmosphere (Ar). For studies using an atomic force microscope, the upper layer of the film with the thickness close to 200 nm was removed, the structure of the film was analyzed at the design depth of ions with the given energy ($R_P = 201$ nm). The image of the surface of sample with Si-nc (Fig. 4) clearly shows the "islands",
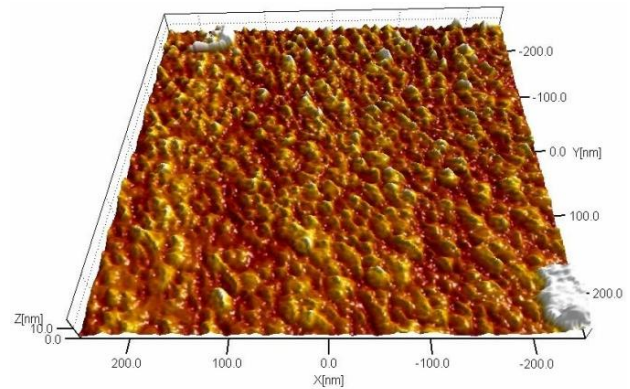
the lateral size of which is approximately 10 nm, and the vertical one less than 4 nm. The density of the nano-clusters in this case is higher than $5 \cdot 10^{11}$ cm^{-2}.
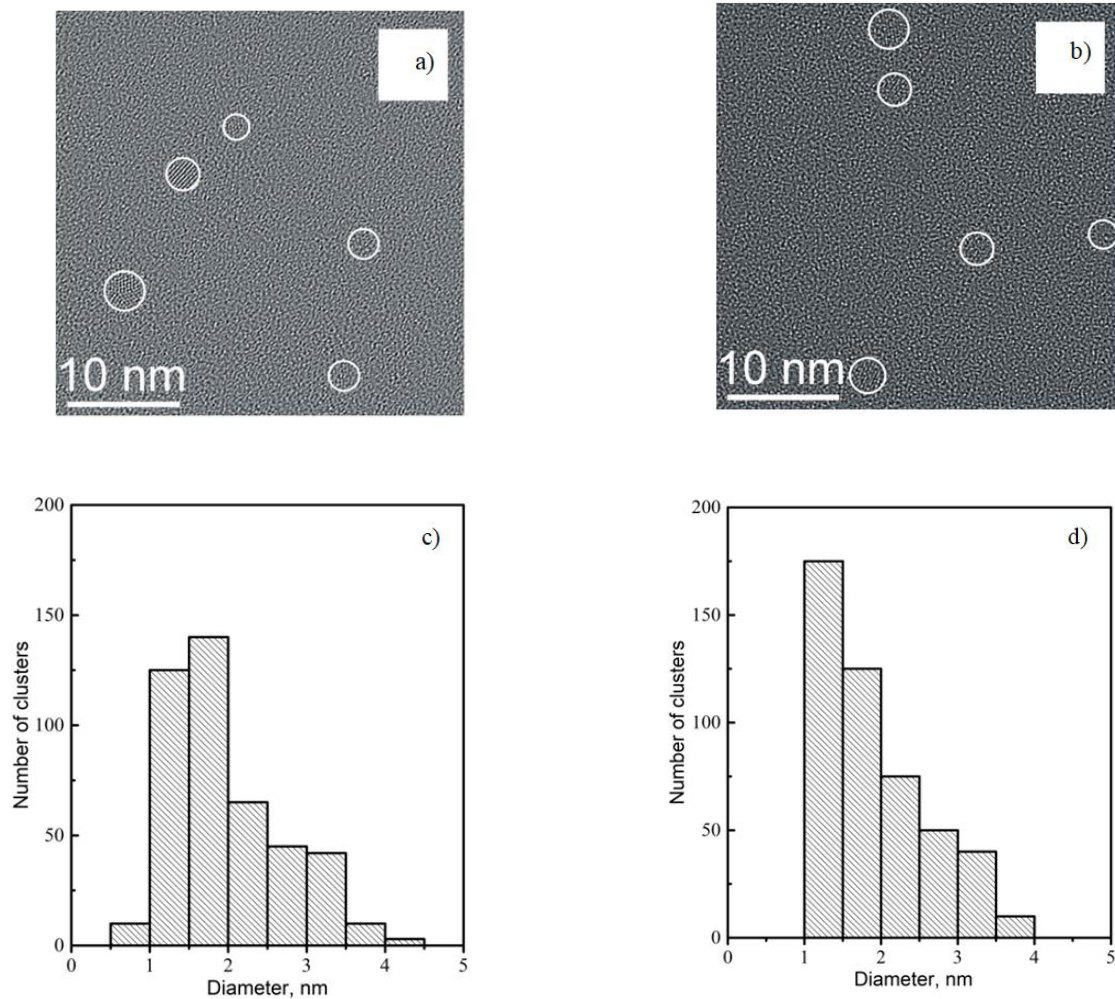
Fig. 5 shows TEM images in the light field at atomic resolution for samples obtained by conventional ion implantation ($E = 100$ keV, $D_{Si} = 8 \cdot 10^{16}$ cm^{-2}) and with ultrasonic treatment ($f = 9.5$ MHz, 1 W/cm^2) after high-temperature annealing ($T_a = 1100$ °C, 20 min, N$_2$).

Spherical silicon nanocrystals embedded into the amorphous matrix are observed. The particle size can be described by the Gaussian distribution with the average size of 1.9 nm and the dispersion of 0.7 nm for control samples and 2.0 nm with the dispersion of 0.7 nm for the samples prepared by ultrasonic treatment.

Analysis of the images in the dark field mode and scanning of the sample showed that the distribution of silicon nanoinclusions is the same for both types of samples and its centroid is located at the distance of 190 nm from the surface, which is close to the design depth of implanted ions.

The images shown in Fig. 5 correspond to the region of the centroid of the distribution of silicon nanoclusters. When the surface density of the nanoclusters for the studied area of the sample was estimated, the value of $\sim 4 \cdot 10^{11}$ cm^{-2} was obtained. This result is consistent with the data obtained using the AFM technique. The difference may be due to the fact that transmission electron microscopy does not provide information about amorphous silicon nanoclusters, which are taken into account in AFM measurements. With account that the annealing temperature of the studied samples was only 1100 °C, it is likely that not all nanoclusters have the crystalline structure [44]. The volume concentration of crystalline nanoinclusions in the design ion range can be calculated using the layer thickness of the investigated film with Si-nc (~ 10 nm), which is $\sim 4 \cdot 10^{17}$ cm^{-3}.

According to the results of transmission electron microscopy, the size and size dispersion of silicon nanocrystallites in the samples prepared using acoustic-

Melnik V.P., Popov V.G., Romanyuk B.M. et al. Luminescent properties of the structures with embedded silicon ...

283

Fig. 5. TEM images at atomic resolution for the samples without (a) and with (b) ultrasonic treatment and the corresponding histograms of the distribution of clusters by size: (c) for control samples, (d) for implanted with ultrasonic treatment. Silicon clusters are highlighted by light circles.
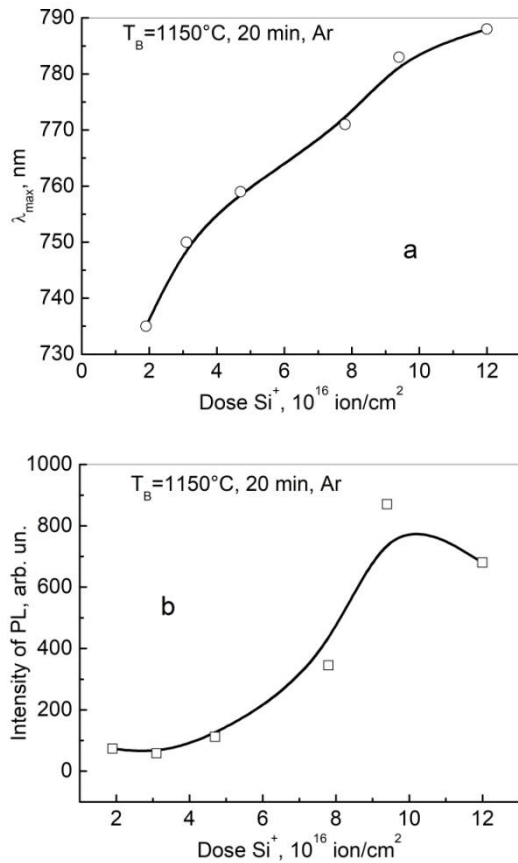
stimulated ion-beam synthesis and conventional ion implantation are almost the same. Although, it should be noted that formation of nanocrystallites (growth) during high-temperature annealing is much faster in the case of acoustic-stimulated synthesis. Depending on the concentration of implanted silicon, temperature, ultrasonic power, *etc.*, the time required to complete formation of the array of nanoclusters is two to four times less for the case of acoustic-stimulated synthesis.

3.3. Photoluminescent properties of the structures with Si-nc

Dependence of PL on the concentration of silicon in the film. PL was observed only for films in which the concentration of excess silicon was more than 2 at.%. This result is consistent with the literature data [29]. As the dose of Si^+ increases, the maximum of the PL band shifts to the long-wave region (Fig. 6a), and the intensity increases and reaches its maximum value at

$D_{Si^+} \sim 9.4 \cdot 10^{16}$ ion (Fig. 6b). The long-wave shift of the position of the PL band maximum with the increasing Si^+ dose, in accord to the quantum-size effect model, is associated with an increase in the average size of nanoclusters. The presence of optimal dose at which the PL maximum is observed also agrees well with this model. In fact, increasing the dose of implanted silicon, on the one hand, leads to the increase in the concentration of Si-nc, and, on the other hand, causes formation of larger nanoclusters. However, the increase in the average size of nanoclusters also causes the deterioration in the conditions of the quantum-size localization and, accordingly, reduces the probability of radiative recombination.

In our case, the PL intensity maximum is observed for samples with the excess silicon concentration close to 10%. Estimation of the average size of Si-nc by the PL band maximum position gives the values of ~ 3.1 nm, which significantly exceed the values obtained with TEM (Fig. 5).

Melnik V.P., Popov V.G., Romanyuk B.M. et al. Luminescent properties of the structures with embedded silicon …

284

Fig. 6. Dose dependence of the PL band maximum position (a) and the PL intensity (b) for SiO$_2$ films (350 nm) implanted with Si$^+$ after annealing at 1150 °C in Ar for 20 min.
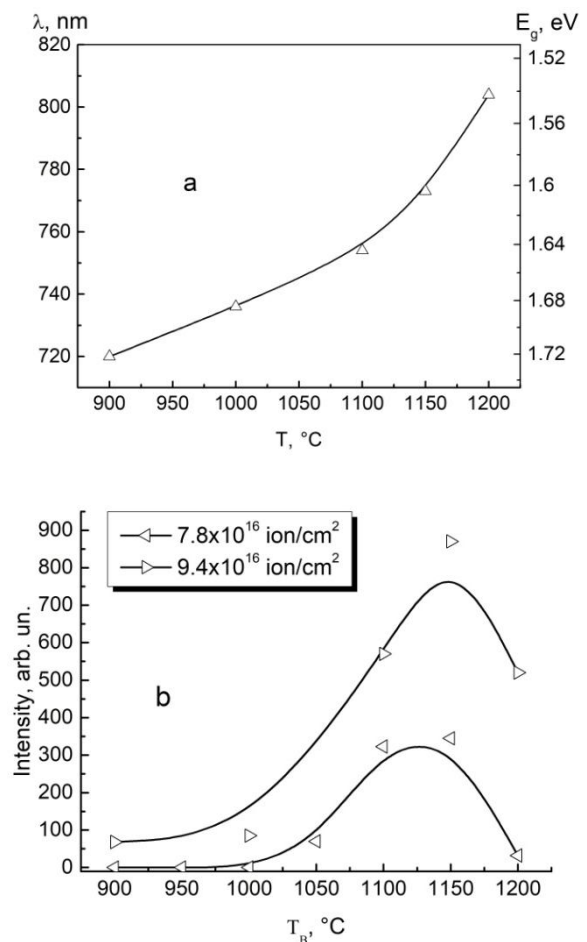
Dependence of PL on the annealing temperature. The intensity of PL also significantly depends on the annealing temperature. The PL intensity maximum was observed after annealing at the temperatures of 1100…1150 °C (Fig. 7b). According to the literature [86], in the annealing temperature range 1100…1200 °C the crystallization process of amorphous nanoclusters is practically completed. There is also the shift of the maximum position into the long-wave region with increasing the annealing temperature.
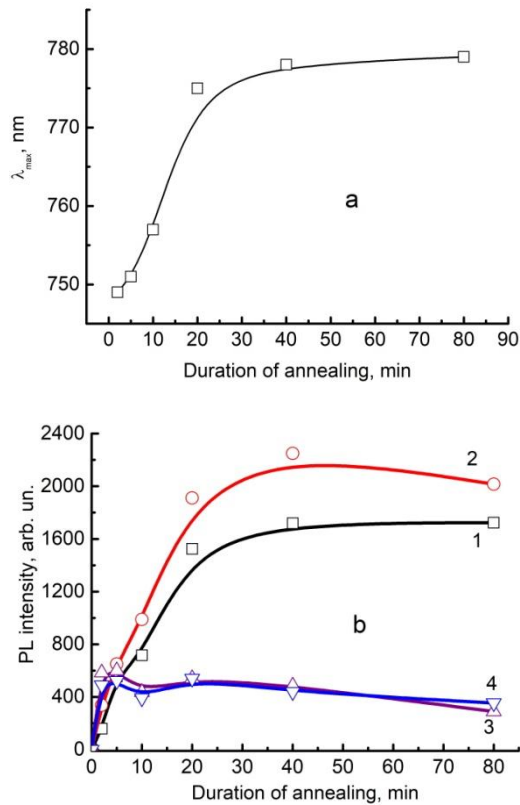
The dependence of the PL on the annealing temperature is consistent with the model of the quantum-size effect. Indeed, the diffusion coefficient of silicon and oxygen increases with increasing the temperature [31, 32], which promotes formation of larger nanoclusters. On the one hand, increasing the size of nanoclusters leads to the shift of the PL maximum into the long-wave region, but on the other hand, to deterioration of the conditions for quantum-size localization. Therefore, at the temperature of 1200 °C there is a decrease in the PL intensity.

According to the quantum-size effect model, the effective band gap of Si-nc can be estimated from the position of the PL band maximum: $E_g = 1240/\lambda_{max}$, where E_g is the band gap in eV, and λ_{max} is the position of the PL band maximum in nm.

Fig. 7a shows the dependence of the PL band maximum position and the band gap on the annealing temperature for the SiO$_{1.5}$ (d = 480 nm) film. The band gap decreases from 1.72 to 1.54 eV with the increase in the annealing temperature from 900 up to 1200 °C. It is possible to estimate the average size of nanocrystals at given annealing temperatures using the experimental data on the relationship between the band gap and the size of Si-nc, given in [44, 87]. In such a way the estimated average size of nanocrystallites increases from 2.4 to 3.4 nm with increasing the temperature from 900 to 1200 °C. The estimated values of the average crystallite size exceed the experimental ones obtained using TEM (2.15 nm) for the structures with the same concentration of excess silicon (~ 10 at.%) obtained with ion implantation. In addition, they exceed the experimental data reported in the literature for structures with Si-nc based on SiO$_x$ films with the same and higher concentrations of Si after similar heat treatments. The reason of this discrepancy is probably application of the quantum-size effect model for interpretation of PL data,

Fig. 7. The dependence of the PL band maximum position of the SiO$_{1.5}$ film (a) and the PL intensity for implanted SiO$_2$ films with the Si excess of 6.7 and 7.8% (b) on the annealing temperature. Annealing in the Ar atmosphere for 20 min.

Melnik V.P., Popov V.G., Romanyuk B.M. et al. Luminescent properties of the structures with embedded silicon …
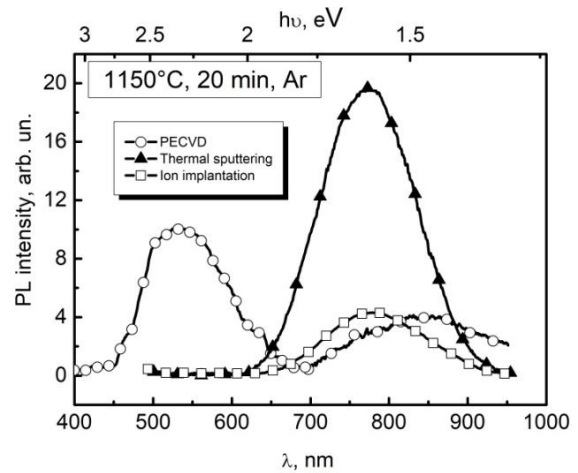
285

Fig. 8. The dependences of the PL band maximum position (a) and the PL intensity (b) of the structures with Si-nc on the duration of annealing in Ar at 1150°C (SiO$_{1.5}$ films).

Fig. 9. PL spectra of SiO$_{1.5}$ films obtained using different methods, after annealing at 1150 °C, in Ar for 20 min.

which gives the clear relationship between the wavelength of emitted light and the band gap and, accordingly, the size of Si-nc. If we use the model of localized electronic states at the SiO$_2$/Si-nc interface to explain the experimental results, the PL data are in full agreement with the data on the structure of the studied samples.

Dependence of PL on the annealing duration. Increasing the duration of annealing from 1 to 20 min leads to the increase in the PL intensity (Fig. 8b), and the position of the PL band maximum is shifted to the long-wave region (Fig. 8a). Further increase in annealing time to 60 min practically does not affect the properties of the studied structure.

For structures with Si-nc obtained by three different methods, we can identify the following common features of PL (Fig. 9): i) the maximum intensity of PL is observed for the films with the silicon concentration of 39-40 at.%; ii) the optimum temperature of heat treatments is ~ 1150 °C; iii) increasing the duration of annealing leads to the increase in the PL intensity, and at a certain time of annealing it reaches saturation (for thermally evaporated film ~ 20 min, implanted – 40 min, deposited by PECVD – 90 min); iv) the PL band in the red and near-infrared regions of the spectrum shifts to the long-wave region with increasing the annealing temperature and silicon concentration in the film.

However, the PL properties of these structures differ significantly (Fig. 8). For the films prepared using the PECVD method, the intense band with the maximum at 560 nm is observed in the PL spectrum, which is not typical for the films obtained using other methods after these heat treatments. Analysis of the elemental composition of the films showed that nitrogen was present in the films prepared using PECVD. If we interpret the presence of two PL bands within the quantum-dimensional effect, we must assume the existence of the array of Si-nc with two characteristic dimensions: ~ 2.2 nm ($\lambda_{max} = 560$ nm) and 4.0 nm ($\lambda_{max} = 800$ nm). However, the TEM results confirm formation only the Si-nc array with the average size of ~ 2.15 nm. It was hypothesized that the short-wave PL band is indeed related to direct recombination in the nanocluster, whereas the long-wave band is due to radiative recombination through the electronic states at the interface between the nanocluster and the dielectric matrix. The presence of nitrogen in this case leads to passivation of broken bonds (centers of nonradiative recombination) and allows to observe the PL band caused by recombination directly in Si-nc.

Since the results of transmission electron microscopy for the studied structures confirm formation of Si-nc, in our opinion, there are three possible approaches to the interpretation of the PL band with a maximum at 560 nm in the films with nitrogen admixture:

1) The presence of nitrogen leads to the fact that part of the nanoclusters is surrounded not by the oxide matrix, but nitride or oxynitride, the PL band with the maximum of 800 nm (1.55 eV) is characteristic for Si-nc in the SiO$_2$ matrix, and the band with the maximum of 560 nm (2.21 eV) is for Si-nc in the Si$_3$N$_4$ matrix (Fig. 10a). This result is consistent with the literature data: the PL band of Si-nc in Si$_3$N$_4$ is shifted to the short-wave region by 0.6 eV relative to the PL band for Si-nc of the same size in SiO$_2$ [23, 88].

Melnik V.P., Popov V.G., Romanyuk B.M. et al. Luminescent properties of the structures with embedded silicon ...

286

2) Nitrogen modifies the Si-nc/SiO₂ interface (passivates broken bonds) and leads to the fact that recombination of electron-hole pairs occurs not only through interface levels (PL band with the maximum of 800 nm), but also directly in the nanocluster (PL band with a maximum of 560 nm) (Fig. 10b). Such an explanation of the presence of two PL bands for structures with Si-nc is found in the literature [7, 89, 90].

3) The presence of nitrogen leads to stabilization of defective complexes, which are responsible for the PL band around 560 nm (Fig. 10c).

The invariance of the position of the PL band with a maximum of about 560 nm with changes of the silicon concentration in the film and the annealing temperature indicates in favor of the third mechanism of radiative recombination in films with nitrogen admixture.

Therefore, the position and intensity of the PL band for structures with Si-nc is determined not only by the concentration of silicon in the original SiO_x film and heat treatment parameters, but also by the technology peculiarities of the film preparation itself.

4. Influence of impurity ion implantation on the properties of structures with Si-nc

In the synthesis of structures with Si-nc by using the method of thermal decomposition of the SiO_x phase ($x < 2$), the radiative properties of nanoclusters are defined by the amount of excess silicon in the original film and heat treatment parameters. Reducing the concentration of the excess Si leads not only to the desired shift of the PL spectrum into the short-wave region, but also to the decrease in the intensity of radiation. Changing the technological parameters for obtaining silicon nanocluster structures does not allow to increase the intensity of PL at the given position of the maximum. The increase in intensity is almost always associated with the shift of the maximum into the long-wave region. Therefore, it is not possible to create the structures with intense PL in the blue and green regions of the visible spectrum. This problem can be solved using introduction of impurities.

4.1. Influence of aluminum and titanium

Introduction of impurities into the studied SiO_x films implies that, due to active interaction with the oxygen, it could change the conditions for Si-nc formation and stimulate the nucleation of Si-nc. This can change both the size of the synthesized nanocrystalline inclusions and PL properties. These impurities during annealing must form chemical bonds with oxygen atoms, thereby changing the conditions for silicon nanoclusters formation.
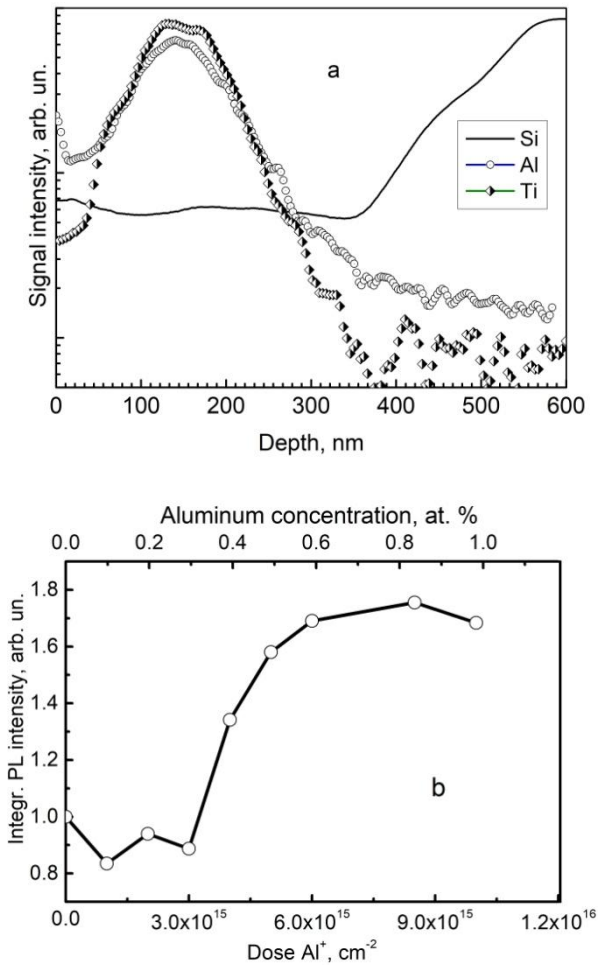
Based on these considerations, studies of the effect of implantation of chemically active metals Al and Ti on the light-emitting properties of the structures with Si-nc were performed. Aluminum and titanium are widely used in microelectronics. At the same time, they have significantly different properties in relation to chemical interaction with silicon and oxygen, which stimulates interest to their study.
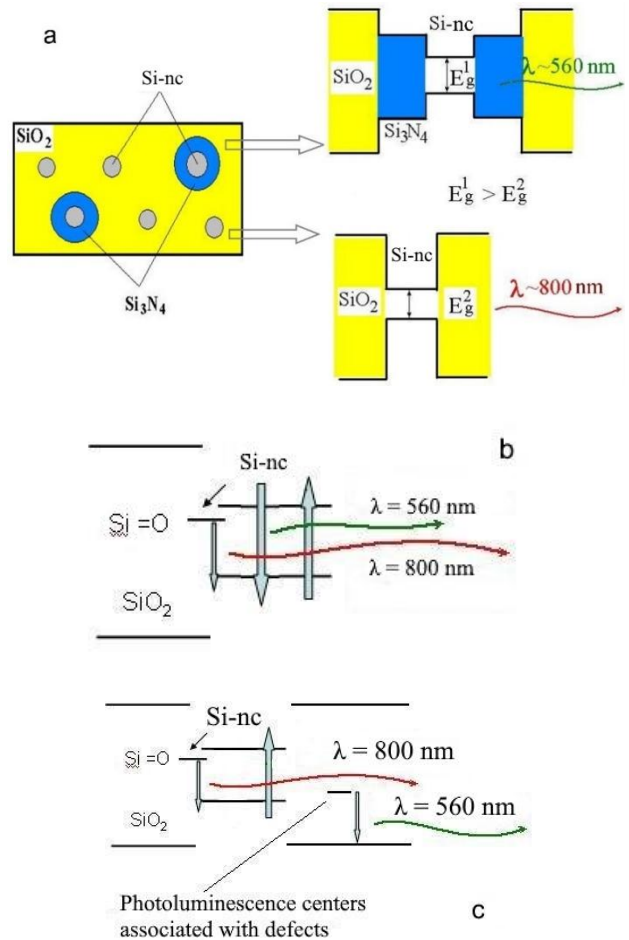
Fig. 10. Mechanisms of radiative recombination in the films doped with the nitrogen impurity.

Aluminum and titanium were introduced into the original film by ion implantation (Fig. 10a). Implantation of the same dose of aluminum and titanium had different effects on the radiative properties of the structures with Si-nc. Implantation of aluminum caused the increase in the PL intensity, while introduction of titanium led to PL quenching. Introduction of the impurities reduced the duration of annealing required to obtain films with optimal light-emitting properties: for implantation of Al – down to 40 min, and for implantation of Ti – down to 20 min.

The effect of aluminum on PL properties of the structures with Si-nc depends on the dose of implanted ions. The depth distribution of Al in $SiO_{1.48}$ film is depicted in Fig. 11a. Fig. 11b shows the dependence of the integrated PL intensity on the dose of implanted Al^+ ions. At low doses, there is some reduction in the intensity of PL as compared with non-implanted samples. This is probably due to the ion-beam disordering of nanoinclusions that exist in the initial (non-implanted) sample. Only at doses of aluminum higher than $3.5 \cdot 10^{15}$ ions/cm², the PL intensity of implanted samples reached the level typical for the initial (non-implanted) sample. The increase in the PL intensity with increasing

Melnik V.P., Popov V.G., Romanyuk B.M. et al. Luminescent properties of the structures with embedded silicon ...

287

Fig. 11. Distribution profiles of the implanted Al and Ti ($D_{Al,Ti} = 8.5 \cdot 10^{15}$ cm^{-2}) in SiO$_{1.48}$ ($d = 426$ nm) film (a) and the dependence of the integrated PL intensity on the dose of the implanted Al after annealing at 1150 °C during 20 min in Ar (b).

the Al dose was observed. The maximum PL intensity was observed for the samples implanted with the aluminum dose of $\sim 8 \cdot 10^{15}$ ions/cm^2. Further increasing the dose of implanted Al$^+$ ions resulted in deterioration of the light-emitting properties inherent to the structures containing Si-nc. Implantation of the aluminum dose of $\sim 1 \cdot 10^{16}$ ion/cm^2, which provided the concentration of ~ 1 at.% at the depth of the average ion path, led to decreasing the PL intensity.

During high-temperature annealing, aluminum atoms mainly react with oxygen atoms, which provides formation of Al–O bonds, while formation of Al–Si bonds is not observed [91]. Since the enthalpy of Al$_2$O$_3$ phase formation ($\Delta H \sim 1657\ldots1676$ kJ/mol) is higher than that of the SiO$_2$ phase formation ($\Delta H \sim 861\ldots911$ kJ/mol) [92, 93], the presence of Al in the film SiO$_x$ results in predominant formation of the Al$_2$O$_3$ phase, and excess silicon takes part in formation of nanoclusters. This process is quite complex, because the mechanisms of diffusion of the impurities play an important role in formation of multiphase systems. Critical parameters are

the concentration of Al and the value of stoichiometry index x. The dose dependence of the PL band intensity in the visible region (Fig. 11b) indicates the presence of optimal dose of aluminum, at which the maximum PL is observed. Taking into account that the optimal dose ($\sim 8 \cdot 10^{15}$ ions/cm^2) provides the concentration of Al at the depth of average range less than 1 at.%, it is possible to assume that the mechanism of the PL increase is not related to the increasing the concentration of additional "released" silicon in the film (< 0.75 at.%), but is caused by the local influence of the presence of aluminum on the process of the SiO$_x$ phase decay.

The decrease in the PL intensity in SiO$_x$ samples implanted with Ti indicates that the mechanism of interaction of Ti with the SiO$_x$ matrix is different than in the case of aluminum. In [94] it was shown that the titanium actively interacts with both oxygen and Si during annealing.

In addition, Al and Ti atoms can get into individual nanocrystallites and form impurity levels in the band gap of Si-nc: Al creates the shallow ones with low recombination activity, Ti forms recombinationally active deep levels, which serve as the centers of nonradiative transitions [95]. Therefore, the implantation of Al can increase the intensity of PL, while the implantation of Ti leads to the decrease in the PL intensity.
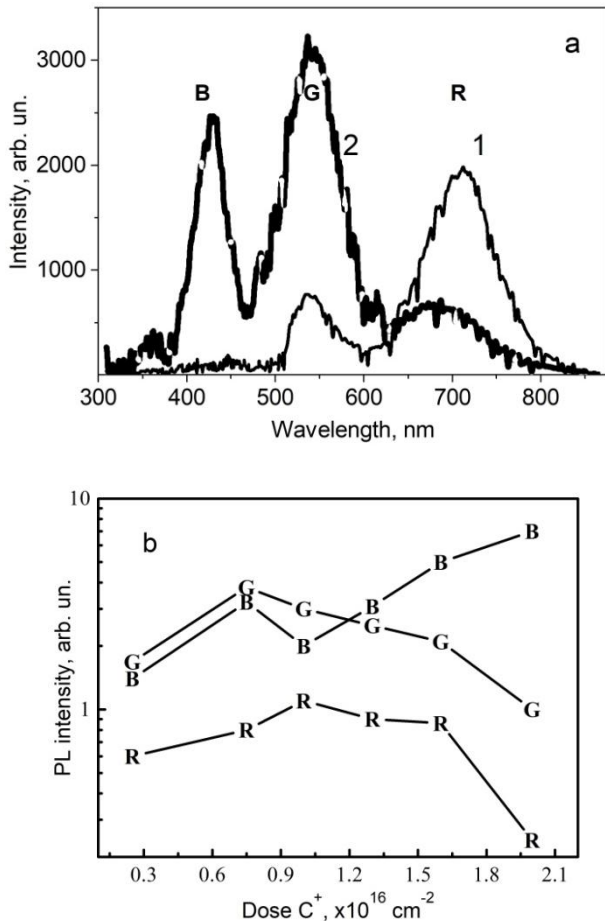
Thus, the difference between the effects of Al and Ti on PL is due to two features: the first, titanium atoms during high-temperature annealing form bonds with both oxygen and silicon, while aluminum interacts only with oxygen atoms; secondly, aluminum atoms, falling into Si-nc, can form shallow impurity levels with low recombination activity, while titanium atoms form deep, recombinantly active impurity levels, which can be centers of non-radiative recombination.

4.2. Influence of carbon implantation

Nitrogen and carbon were detected in the studied samples, which affected the light-emitting properties of Si-nc. Taking into account the probability of the presence of carbon impurities in the initial SiO$_x$ films, it was decided to find out how the implantation of C affects the formation process and the properties of structures with silicon nanoclusters. On the other hand, the literature data show that the implantation of carbon can significantly expand the range of wavelengths emitted by the nanocluster structure based on silicon [68, 69].

For the objective study of the mechanisms of the influence of carbon on the formation process and light-emitting properties of structures with silicon-based nanoclusters, two approaches were used to obtain SiO$_x$ films with carbon admixture: the implantation of silicon and carbon in silicon dioxide films and the implantation of oxygen and carbon in a silicon substrate.

Implantation of silicon and carbon in SiO$_2$ films. SiO$_2$ films obtained by thermal oxidation of the silicon wafer were implanted with silicon ions ($E = 100$ keV and $D_{Si} = 6 \cdot 10^{16}$ cm^{-2}) to form the SiO$_x$ suboxide film.

Melnik V.P., Popov V.G., Romanyuk B.M. et al. Luminescent properties of the structures with embedded silicon …

288

Fig. 12. PL spectra of the samples implanted with silicon ions (*1*), and silicon and carbon ions ($D_C = 1 \cdot 10^{16}$ cm^{-2}) (*2*) (a) and the dependence of PL intensities for different spectral peaks on the dose of additionally implanted carbon (b), after annealing in Ar at $T = 1100$ °C for 15 min.

The maximum concentration of silicon in the film at the depth of the projective run was ~ 37-38%. At the next stage, carbon implantation was performed with the parameters that ensured the coincidence of the distribution profiles of Si and C in the SiO$_2$ film ($E = 50$ keV and $D_C = 2.5 \cdot 10^{15} \ldots 2 \cdot 10^{16}$ cm^{-2}).

Implantation of Si ions only results in the broad band with the maximum at 700 nm and the low-intensity band with a maximum at 540 nm (Fig. 12a, curve *1*). In the samples after combined implantation of Si$^+$ + C$^+$ intensive PL bands with maxima at 425 nm, 540 nm, PL band in the region of ~ 680 nm, as well as low-intensity band with the maximum at 360 nm are observed (Fig. 12a, curve *2*). These bands (except for the 360 nm band) are denoted for convenience as R, G and B with the maxima at ~ 700, 540 and 425 nm, respectively. The dependences of PL intensities for different spectral peaks on the dose of additionally implanted carbon are shown in Fig. 12b.
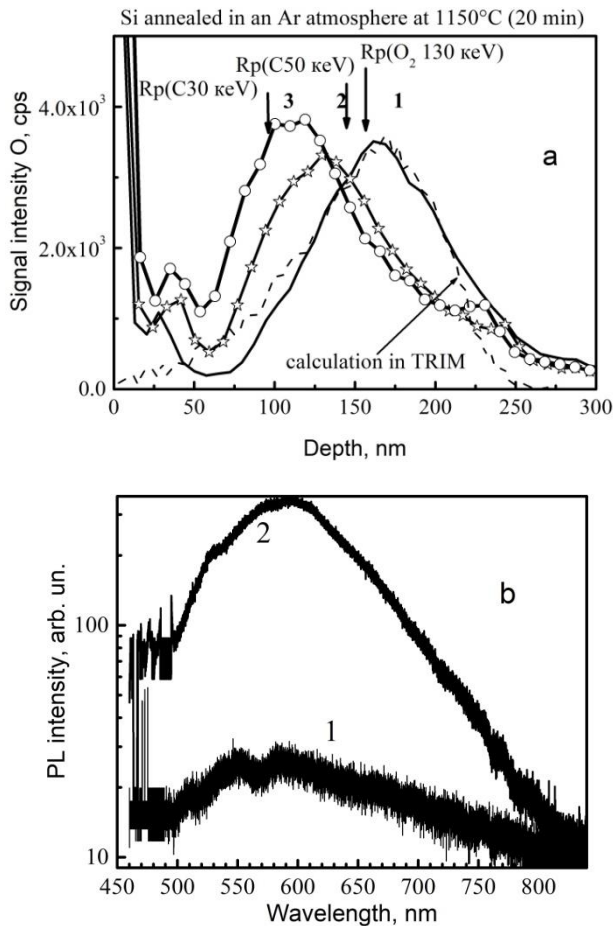
The obtained results cannot be explained exclusively by using the model of quantum-size effects in nanocrystalline silicon. This model is acceptable partly

for the R-band. The R-band occurs at annealing temperatures higher than 1050 °C. Its energy position after annealing at the temperature of 1100 °C indicates that the average size of Si nanocrystals is ~ 3 nm [44]. The estimated values of the average crystallite size exceed the experimental values obtained by TEM ~ 2 nm (Fig. 5), which may indicate the feasibility of considering localized electronic states at the interface SiO$_2$/Si-nc when describing light-emitting properties. Increasing the annealing temperature to 1200 °C leads to the shift of this band into the long-wave region, which is associated with the increase in the size of nanoclusters.

The decrease in the band intensity at these temperatures indicates the decrease in the concentration of nanocrystals due to the increase in their size and deterioration of the conditions for quantum-size localization. The presence of the carbon slows down the process of Si precipitation by creating Si–C bonds and reducing the diffusion coefficient of silicon [96]. In the structures implanted with carbon, the R-band is shifted to the short-wave region, which indicates the decrease in the size of Si nanoclusters.

The intensity of G-band reaches its maximum at low annealing temperatures, when nanocrystallites are not formed. The energy position of the G-band depends on the carbon dose and annealing temperature, and the band itself consists of two components. The low-energy component that dominates at high concentrations of carbon is likely to be associated with the carbon clusters. In our opinion, the higher-energy component, which dominates at temperatures of 600 up to 800 °C, is associated with the step-like silicon-containing structural formations such as organosilicon compounds. Indeed, as shown in [97], organosilicon polymers with Si–C bonds, as well as polymeric compounds, namely siloxenes, which include oxygen have similar to low-size silicon objects (nanoclusters, nanowires and quantum layers) properties. The organosilicon compounds can have different structures: one-dimensional chains, branched, stepped, and reticulate or planar-siloxene. The spectral position of the high-energy component of the G-band coincides with the position of the photoluminescence band for silicon-containing polymers with the step-like structure that are stable up to the temperatures close to 800 °C [97]. The presence of a PL band with the maximum at 360 nm indicates creation of small number of the chain silicon formations, the nature of the luminescence of which is associated with delocalized excitons [98].

The energy position of B-band is close to that observed when studying porous silicon carbide PL [99]. If we take into account that the energy of Si–Si, Si–C and C–C bonds is 2.36, 3.21 and 3.70 eV, respectively, then with increasing the annealing temperature thermo-dynamically favorable is formation of carbon and SiC nanoclusters. It corresponds to the obtained results according to which the higher intensity of the G- and B-bands is observed for high annealing temperatures.

Melnik V.P., Popov V.G., Romanyuk B.M. et al. Luminescent properties of the structures with embedded silicon ...

Fig. 13. Oxygen distribution profiles of samples implanted with oxygen (*1*) and additionally with carbon ions possessing the energies of 50 keV (*2*) and 30 keV (*3*) (a) and PL spectra for samples implanted with oxygen (*1*) and co-implanted with carbon (b), after annealing in Ar at *T* = 1150 °C for 20 min.

The presence of the R-band at these temperatures is explained by the fact that the concentration of implanted silicon by several times exceeds the concentration of carbon, and at formation of carbon nanoclusters the excess silicon precipitates in the form of the nanocrystals.

It should be noted that at the annealing temperature of 1000 °C there is the sharp drop in the intensity of G- and B-bands, which may be caused by the processes of restructuring (nucleation of Si-nc) and increasing the concentration of broken bonds, which are the main channel for nonradiative recombination [100].

Therefore, implantation of carbon into SiO$_x$ films leads to formation of carbon and silicon carbide nanoclusters and silicon-containing polymers with a step-like structure along with the Si-nc, which results in significant expansion of the wavelength range of light emitted by these structures.

Implantation of oxygen and carbon into the silicon substrate. When forming buried SiO$_2$ films in the case of known SIMOX (silicon implanted with oxygen) technology, these films contain inclusions of silicon crystallites. As a rule, the size of these crystallites is within

the range of 10 to 100 nm and their use for light emission is impossible. However, creation of buried dielectric layers with silicon nanocrystals has the prospect of practical application in multilevel optoelectronic circuits.

Creation of a buried layer of SiO$_2$ in silicon is accompanied by generation of the large number of defects and significant mechanical stresses, which remarkably complicates the process of SiO$_2$ phase formation and stimulates creation of dislocation loops. Reduction of the mechanical stresses in such structures is possible through generation of vacancies. Carbon is the widely used impurity to generate vacancies in silicon. During annealing, carbon implanted into silicon forms the network of vacancies in silicon, which is the drain for interstitial silicon atoms. Therefore, additional implantation of carbon in the area between the generated buried oxide (BOX) structure and the surface stimulates formation of SiO$_2$ phase and reduces the concentration of unwanted defects (dislocations and dislocation loops) and promotes formation of crystalline silicon nanoclusters in this area.

Silicon wafers were implanted with oxygen ions O_2^+ (E = 130 keV and $D_{O_2} = (1.8...5) \cdot 10^{17} \, cm^{-2}$) to form the suboxide SiO$_x$ film. The maximum concentration of oxygen in the film at the depth of the design run is $\sim (1.1...3.0) \cdot 10^{22} \, cm^{-3}$. At the next stage, carbon implantation was performed. Implantation of carbon was carried out in two modes: i) carbon implantation in the region of maximum oxygen concentration (coincidence of the distribution profiles O and C in Si) at conditions E = 50 keV and $D_C = 2 \cdot 10^{16} \, cm^{-2}$; ii) implantation of carbon in the area between the created hidden SiO$_2$ layer of and surface (E = 30 keV and $D_C = 1 \cdot 10^{16} \, cm^{-2}$). The parameters of heat treatments and details of experiment see in [101].

The oxygen distribution profile coincides with that theoretically calculated using the TRIM program in the samples after oxygen implantation (Fig. 13a, curve *1*). After additional carbon implantation, the oxygen distribution profile is shifted toward the sample surface, and it is in the region between the maximum carbon distribution at the given energy and the concentration maximum of the vacancies created during oxygen implantation (Fig. 13a, curves *2* and *3*).

The region with the thickness close to 30 nm with the constant oxygen concentration is observed in the samples implanted with carbon at the energy of 30 keV, which indicates creation of the thin stoichiometric SiO$_2$ layer.

In the case of additional carbon implantation, the nucleation of the SiO$_2$ phase takes place in the region of carbon distribution, and the oxygen distribution profile is shifted to the surface. This is caused by two factors: i) in the region of carbon distribution, the critical radius of SiO$_2$ precipitates is much smaller, which creates conditions for effective formation of the SiO$_2$ phase; ii) there are no drains for interstitial atoms, which reduces the rate of precipitation in the initial distribution of oxygen.

Melnik V.P., Popov V.G., Romanyuk B.M. et al. Luminescent properties of the structures with embedded silicon ...

290

In our opinion, PL is associated with the presence of nanocrystalline silicon inclusions with the size of 2 to 5 nm in the thin stoichiometric SiO_2 layer, which was formed in the samples implanted with oxygen and carbon. The presence of these inclusions is confirmed by the results of diffuse X-ray scattering [102].

Therefore, additional implantation of carbon ions into silicon structures implanted with oxygen ions leads to redistribution of oxygen over the thickness and stimulates the emergence of the SiO_2 phase in the region with the maximum carbon concentration. The maximum effect is observed when the carbon distribution profile coincides with the maximum vacancy distribution. The thin (~ 30 nm) stoichiometric layer of silicon dioxide is created in this region. Carbon implantation enables to effectively control formation of silicon nanoclusters and the growth of SiO_2 phase during annealing. After annealing of the samples additionally implanted with carbon, PL with the peak at 600 nm is observed (Fig. 13b), this is associated with inclusion of silicon in the thin stoichiometric SiO_2 layer.

When carbon is introduced into SiO_x films, in which there are no significant mechanical stresses during annealing and no formation of Si-nc, formation of carbon and silicon carbide nanoclusters and silicon-containing polymers is observed, which is accompanied by expansion of the wavelength range of emitted light. When carbon is implanted into the region of the buried SiO_x layer obtained by implantation of oxygen in the silicon wafer, formation of silicon nanocrystallites during annealing occurs under significant mechanical stresses. In this case, there observed is thickness redistribution of oxygen and more efficient formation of stoichiometric SiO_2 with embedded Si-nc. That is, in the first case (low mechanical stresses) carbon is the "building material" providing formation of nanoscale inclusions (SiC, carbon nanoclusters), in the second case (when significant mechanical stresses are present) carbon plays the role of "catalyst" promoting formation of SiO_2 phase with embedded Si-nc and compensates significant mechanical stresses that occur in the film.

4.3. The effect of nitrogen introduction

All the above results were obtained for the structures after annealing in the inert atmosphere (Ar). However, in the samples obtained by the PECVD method, the small concentration of nitrogen was revealed, which probably led to significant differences in the photo-luminescent properties of Si-nc structures obtained using this method.

Despite intensive researches [64–67], the mechanism of nitrogen effect on the luminescent properties of silicon nanoclusters in the SiO_2 matrix has not been definitively ascertained. To study the effect of nitrogen on the light-emitting properties of the structures with Si-nc, it is important to control the introduction of nitrogen, which can be provided only by ion implantation.
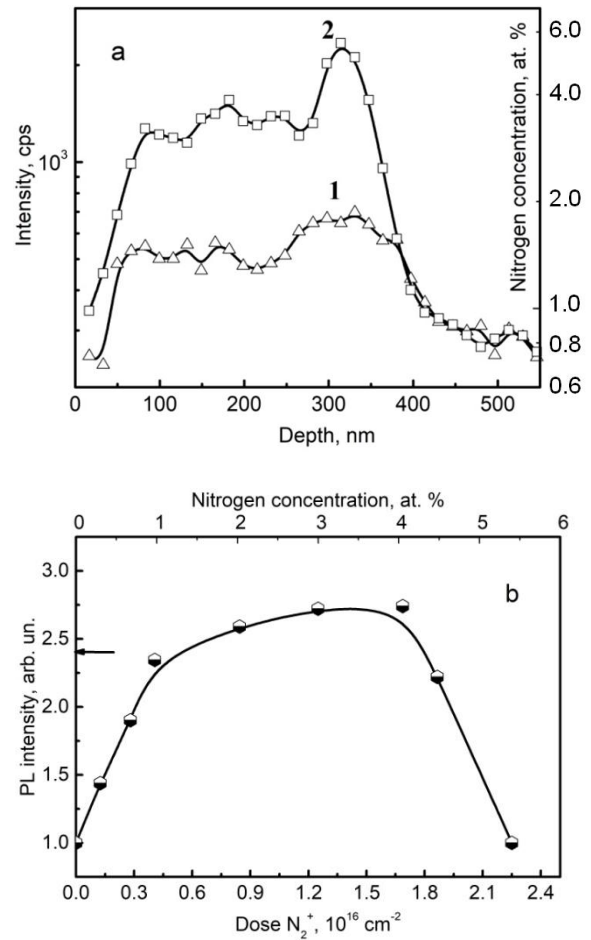
Fig. 14. (a) Nitrogen distribution profiles in $SiO_{1.5}$ films annealed in the N_2 (1) atmosphere and in Ar atmosphere after N_2^+ implantation, $D = 2.2 \cdot 10^{16}$ ion/cm^2 (2) and (b) dependence of PL intensity on the dose of implanted nitrogen after annealing in Ar (the arrow shows the PL of the $SiO_{1.5}$ film annealed in N_2). Annealing at $T = 1150$ °C for 20 min.

During studying the effect of nitrogen on the light-emitting properties of the structures with silicon nanoclusters, nitrogen was introduced into the SiO_x film by using two methods: (i) by thermal annealing in N_2 and (ii) by implantation of N_2^+ ions (see [103] for experimental details).

Uniform distribution of the nitrogen over the thickness of the sample is provided by its diffusion (Fig. 14a, curve 1). The increase in the nitrogen concentration at the depth of ~ 340 nm is due to its ability to accumulate at the SiO_2/Si interface. In case of ion implanted samples, the distribution of the nitrogen atoms along the depth of the sample should be non-uniform (in the form of two Gaussians with maxima at the depths 120 and 240 nm, which correspond to two energies of implantation). However, due to diffusion, the distribution of nitrogen in the implanted samples after annealing becomes almost uniform (except for the region near the SiO_2/Si interface).

Melnik V.P., Popov V.G., Romanyuk B.M. et al. Luminescent properties of the structures with embedded silicon …

291

It was found that the presence of nitrogen increases the intensity of PL (Fig. 14b) and leads to the shift of the PL band in the short-wave region [104]. The effect of the nitrogen on PL does not depend on the method of its introduction, but is defined by the concentration of nitrogen in the film. The use of the ion implantation enables to estimate the required nitrogen concentration, at which the maximum increase in PL intensity is observed. For the structures, in which the excess concentration of silicon is ~ 10 at.%, this optimal dose of nitrogen is within the range of 3.5 to 4 at.%.

To elucidate the mechanism of the annealing atmosphere on the radiative properties of the structures with Si-nc, in addition to annealing in the inert atmosphere and the nitrogen atmosphere, combined annealing was performed: short-term (2 min) and long-term (18 min) with different sequence of annealing atmospheres. It was found that the position of the PL band is defined mostly by the conditions at the initial stage of the annealing, and the intensity is related to the environment of the structure at the final stage of annealing.

The obtained experimental results cannot be explained only within the frames of the quantum-size model, so for their interpretation the PL model with localized electronic states at the SiO_2/Si-nc interface was considered: exciting light is absorbed in nanoclusters, and radiative recombination occurs through the energy levels at the SiO_2/Si-nc interface.

Since the enthalpy of silicon nitride phase formation is significantly lower [92, 93] than the enthalpy of silicon dioxide formation, Si–N bonds are rapidly formed during thermal annealing, and it causes redistribution of the silicon bonds, which slows down the diffusion of silicon in SiO_x film. Thus, at the initial stage of Si-nc formation, the diffusion-limited stage of cluster growth is restricted, and the processes of clusters oxidation are suppressed due to the autocatalytic mechanism [105].

Therefore, the presence of nitrogen stabilizes the SiO_2/Si-nc structure and maintains the high concentration of nanoclusters. During the annealing process, nitrogen is accumulated at the oxide/Si-nc interfaces and passivates the broken silicon bonds, which leads to the decrease in the number of non-radiative recombination centers [106]. Thus, in the process of thermal annealing in nitrogen, the high concentration of nanoclusters surrounded by the SiO_2 phase is maintained, in which the broken bonds are passivated by nitrogen.

The intensity of the PL decreases sharply with increasing the nitrogen concentration from 4 to 5.5 at.% (Fig. 14b). This is caused by occurrence of silicon oxynitride phase at the cluster surface, which decreases the concentration of radiating interface electronic states and, accordingly, decreases the intensity of radiative recombination.

The study of the nitrogen effect on PL of the structures with Si-nc formed by nitrogen implantation in structures with already formed nanoclusters did not

provide direct evidence that the mechanism of nitrogen effect is to modify the interface and create the centers of the radiative recombination. The main obstacle in this case was generation of the large number of radiation defects. These defects significantly reduce the intensity of PL and do not allow to directly study the effect of nitrogen on PL of the structures with Si-nc. However, the obtained results of intensity reduction and short-wave shift of the PL band maximum can be unambiguously explained only in the framework of the model of nitrogen modification of the Si-nc/SiO_2 interface.

Investigation of the nitrogen effect on the light-emitting properties of SiO_2 films implanted with Si^+ showed that the effect of annealing in the nitrogen atmosphere (increase in PL intensity and shift of the PL band maximum position) depends on the concentration of excess silicon in the film [76].

5. Photoluminescence of the structures with Si-nc obtained by acoustic-stimulated ion implantation

The nucleation of the nanoclusters can be stimulated through the use of the ultrasonic treatment of the wafer in the process of the ion implantation. It is known that vacancy complexes are effectively formed during ultrasound treatment at implantation [78, 79], which should facilitate the process of the silicon precipitation in the initial stages of annealing. TEM data confirm formation of the array of nanoclusters with approximately the same sizes and almost the same concentration at both conventional implantation and that with ultrasound treatment (Fig. 4). However, the intensity of the long-wave PL band (1.55 eV) in the samples synthesized with ultrasonic treatment is significantly lower (Fig. 15a). This effect could be associated with the decrease in the concentration of large nanoclusters (4 nm). However, according to the electron microscopic studies, the number and size of nanoclusters in samples obtained with and without ultrasonic treatment is almost the same.

Since the PL band 1.5…1.6 eV, according to [7, 89, 90], can also be associated with recombination through electronic states at the nSi-nc/SiO_2 interface, to discriminate the possible mechanisms of influence of the ultrasonic treatment on the PL intensity, the X-ray photoelectron spectra of these structures has been investigated (Fig. 15b).

The decomposition of X-ray photoelectron spectra into elementary components, according to the procedure described in [77], demonstrates the presence of five elementary components in the Si-2p spectrum, which correspond to the different degrees of silicon oxidation in the matrix.

Table 1 shows the calculated relative integrated intensity of the oxidation state of silicon. The Si^0 component corresponds to the unoxidized silicon (nanoclusters), Si^4 to fully oxidized silicon (SiO_2 matrix), and other components to intermediate oxidation states.

Melnik V.P., Popov V.G., Romanyuk B.M. et al. Luminescent properties of the structures with embedded silicon …

292

Table 1. The relative integrated intensity of the silicon oxidation state.

	Si^0	Si^{1+}	Si^{2+}	Si^{3+}	Si^{4+}
with ultrasound	9.48%	1%	0%	0%	89.52%
without ultrasound	9.6%	3.27%	1.55%	6.25%	79.33%
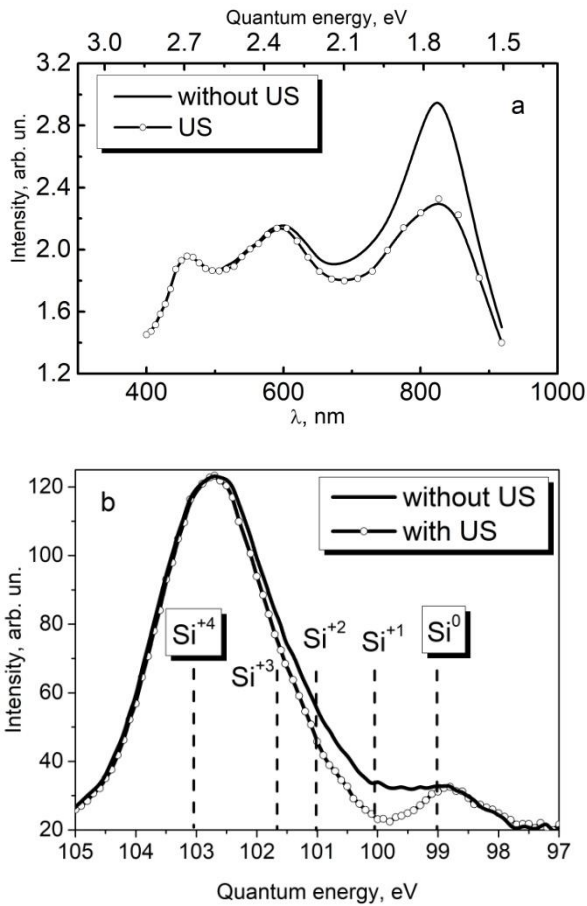
Fig. 15. PL spectra (a) and X-ray photoelectron spectroscopy data (b) for Si-nc structures obtained using ion implantation with and without ultrasonic treatment.

Fig. 16. Dependence of the total content of suboxide states (a) and the intensity of the PL band with the maximum near 800 nm (b) on the power of ultrasonic treatment for structures with Si-nc obtained using acoustic-stimulated ion-beam synthesis.

X-ray photoelectron spectroscopy (XPS) data show that in the case of ultrasonic treatment, the Si-nc/SiO$_2$ interface is more perfect (practically absent 1-, 2- and 3-fold oxidized silicon). In the case of ultrasonic treatment, there is the significant decrease in the intensity of the PL band with the maximum at 800 nm. That is, the decrease in the "transitional" suboxide layer at the interfaces between the Si nanocluster and SiO$_2$ is accompanied by the decrease in PL.

Fig. 16 shows the dependence of the total concentration of silicon suboxide states Si^{n+} (n = 1 to 3) (*a*) and the intensity of the PL band with the maximum near 800 nm (*b*) on the power of the applied ultrasonic wave. The PL band intensity at 800 nm and the total concentration of suboxide states decrease with increasing the ultrasonic processing power.

Taking into account that the average size of Si-nc and their size distribution does not change during ultrasonic treatment (Fig. 5), the similar nature of the dependences of PL intensity and concentration of suboxide states on the applied power of ultrasonic waves indicates that the band in the region of 800 nm related to suboxide states at the Si-nc/SiO$_2$ interface.

Melnik V.P., Popov V.G., Romanyuk B.M. et al. Luminescent properties of the structures with embedded silicon ...

293

In our opinion, when forming the nanocluster structures without ultrasonic treatment, the large amount of underoxidized silicon creates the large concentration of the electronic states at the Si-nc/SiO$_2$, which are responsible for PL in the region of 1.55 eV. Ultrasonic treatment, reducing the concentration of surface electronic states, leads to the decrease in the intensity of the low-energy PL peak, without affecting the higher-energy peaks (Fig. 15a).

Thus, experimental results show that, for the PL band in the red and near-IR regions, the dominant mechanism of radiative recombination is recombination through localized states at the Si-nc/SiO$_2$ interface.

6. Influence of the low-temperature treatments on the light-emitting properties of the structures with Si-nc

Experimental results show that the radiative properties of structures with Si-nc significantly depend on the state of the Si-nc/SiO$_2$ interface. The results of studies of the macroscopic interface Si/SiO$_2$ indicate that its properties can be significantly changed by heat treatment at the temperatures 450 to 850 °C [105, 106].

Low-temperature (LT) annealing of the structures with formed Si-nc at the temperature of 450 °C in vacuum or in the atmosphere of inert gas (Ar) practically does not change the PL spectrum (Fig. 17) [75–77]. At the same time, annealing in the oxygen atmosphere slightly increases the intensity of PL, while the shape of the spectrum does not change. Subsequent LT treatments in N$_2$ atmosphere lead to the significant increase in the PL intensity. In addition, the shape of PL band itself changes – the noticeable shoulder appears in the long-wave region.

The highest PL intensity is observed for the structures that after high-temperature annealing were subjected to LT treatment in the mixture of nitrogen and oxygen. In this case, there is a significant shift of the PL maximum to the long-wave region.

The intensity of PL increases with increasing the period of annealing in air up to 6 hours Note that the position of the PL band is shifted to the long-wave region with increasing the duration of LT annealing. When this period is longer than 6 hours, the intensity of PL goes to the saturation. During long LT annealing in the nitrogen atmosphere, the PL intensity is lower by several times and reaches saturation at the annealing time longer than 1 hour (Fig. 17, insert).

Subsequent thermal annealing at the temperatures above 450 °C leads to the decrease in PL, and repeated modification annealing in the N$_2$ + O$_2$ mixture at 450 °C restores the radiative properties of the structure with Si-nc (for details see [75]).

For the samples formed in the Ar atmosphere, the PL intensity after LT annealing increases more than in the case of the structure formed in the N$_2$ atmosphere.

The highest PL intensity is observed for the structures with Si-nc formed during high-temperature annealing in Ar, which then underwent additional heat treatment in the mixture of nitrogen and oxygen at 450 °C and subsequent passivating annealing in hydrogen (see [76]). For these structures PL is more than an order of magnitude higher than the structures immediately after formation (Table 2).

The integrated PL intensity in normalized on the PL intensity for the structures formed in the Ar atmosphere.
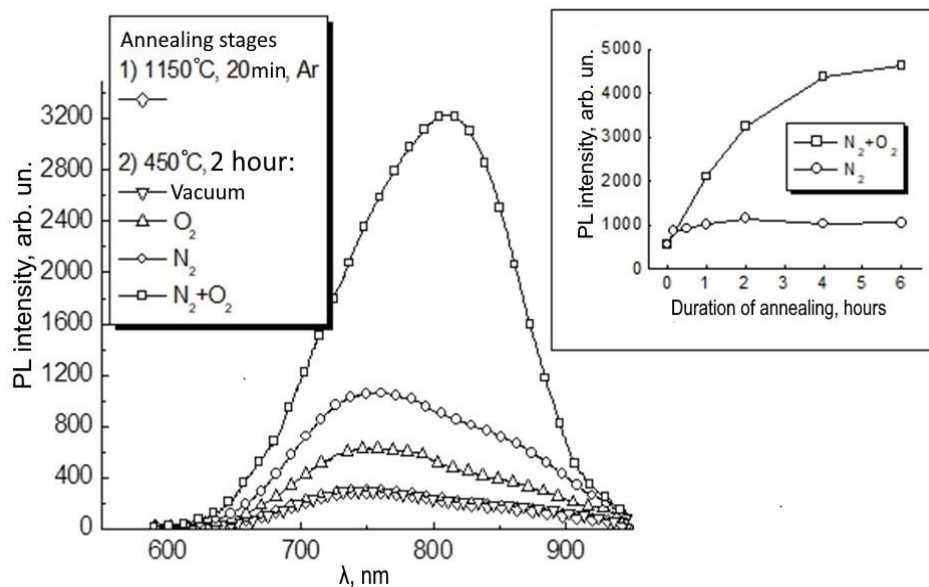
Fig. 17. PL spectra of SiO$_{1.5}$ films after forming high-temperature annealing and subsequent low-temperature annealing in different atmospheres. In the insert – the dependence of PL intensity on the duration of low-temperature annealing in the mixture of N$_2$ + O$_2$ and nitrogen.

Melnik V.P., Popov V.G., Romanyuk B.M. et al. Luminescent properties of the structures with embedded silicon ...

294

Table 2. Integrated PL intensity.

Formation		Low-temperature treatments		
atmosphere	1100 °C	450 °C ($N_2 + O_2$)	480 °C (H_2)	450 °C ($N_2 + O_2$) + 480 °C (H_2)
Ar	1	9.02	6.90	16.83
N_2	1.78	6.59	8.62	8.78

Table 3. Relative integrated intensity of silicon oxidation before and after low-temperature treatment.

	Si^0 (%)	Si^{1+} (%)	Si^{2+} (%)	Si^{3+} (%)	Si^{4+} (%)
I) forming annealing: 1150 °C (Ar)	8.9	1.9	4.0	0	85.3
II) the following NT treatment: 1150 °C (Ar) + 450 °C ($N_2 + O_2$)	6.5	1.1	10.3	0	82.1

The integrated PL intensity in normalized on the PL intensity for the structures formed in the Ar atmosphere.

The results of layer-by-layer analysis of thermally evaporated $SiO_{1.5}$ films after each stage of three-stage annealing: I – 1150 °C (Ar, 20 min); II – 450 °C ($N_2 + O_2$, 2 hours); III – 1150 °C (Ar, 20 min) indicate that nitrogen diffuses into the film during the LT stage (Fig. 18a). After forming high-temperature annealing (I) in the Ar atmosphere, the nitrogen concentration in the film is negligible. But there is some increase in the concentration of the nitrogen at the film-substrate interface, which is associated with its ability to accumulate at the interface. After LT annealing in the mixture of nitrogen and oxygen (II), the concentration of nitrogen in the film increases significantly. Subsequent high-temperature annealing (III) removes nitrogen from the film.

Fig. 18b shows X-ray photoelectron spectra of Si-2*p* for the samples after forming annealing (upper curve) and after subsequent LT treatment (lower curve) and their decomposition into elementary components corresponding to the different degrees of silicon oxidation in the matrix. Table 3 shows the calculated relative integrated intensity of the oxidation state of silicon.
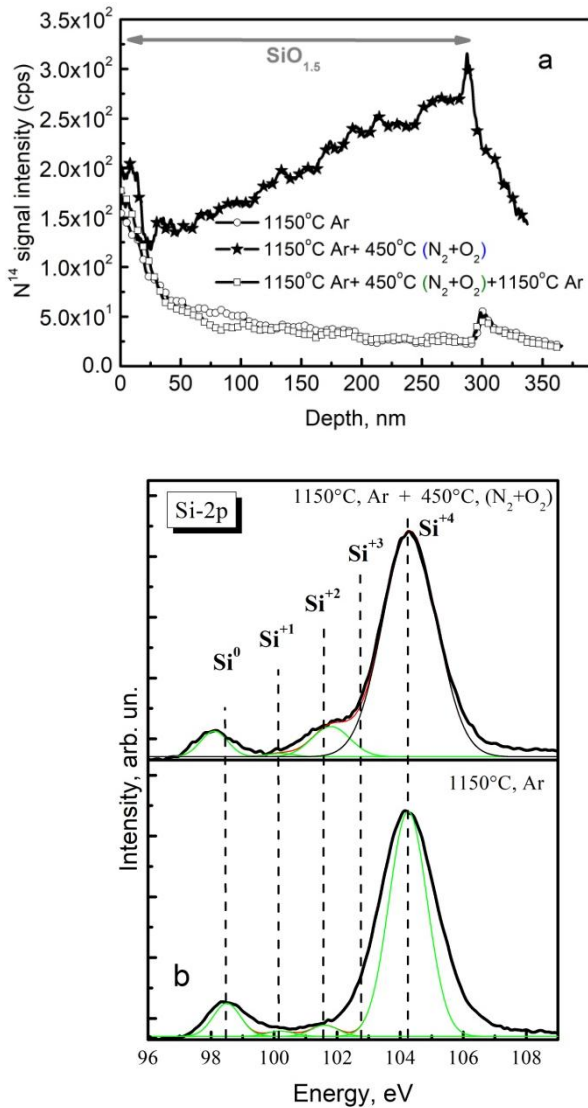
XPS data show that after LT treatment, the "transition" layer at the Si-nc/SiO_2 interface significantly increases (the amount of 2-fold oxidized silicon increases significantly). There is the significant increase in the intensity of PL band with the maximum near 800 nm, namely in this case. That is, the increase of the "transition" layer at the interface between the nanocluster and SiO_2 is accompanied by the significant increase in the PL intensity.

The mechanism of the influence of the LT annealing in $N_2 + O_2$ on PL is related to the reconstruction at the Si-nc/SiO_2 phases interface due to the quasi-chemical reactions involving oxygen and nitrogen atoms [107]. The important factor in the course of quasi-chemical reactions is the presence of broken bonds at the interface, which, in our opinion, is the beginning of the reconstruction of the interface. Measurements of the distribution of nitrogen along the depth of the film showed that nitrogen in the process of LT annealing is distributed uniformly over the entire thickness of the film. Subsequent high-temperature annealing leads to the release of the nitrogen from the film. These experiments indicate that the long-wave shift of the PL band is associated with the reconstruction at the Si-nc/SiO_2 interface and formation of electron energy states through which radiative recombination occurs. XPS data confirm the significant increase of the "transition" layer at the Si-nc/SiO_2 interface after LT treatment.

The kinetics of the process indicates that oxygen, which diffuses into the film, is involved in formation of PL centers (see Fig. 17, insert). Since the oxygen diffusion coefficient at the temperature near 450 °C is quite low [31], the process of formation of these centers is slow. In the case of annealing in nitrogen, there is the rapid process of non-radiative recombination centers passivation by attaching nitrogen to the broken bonds at the nanocluster/matrix interface, then with additional oxygen diffusion new centers are created by oxidation of silicon and autocatalytic maintenance of this reaction with the following bounding of nitrogen.

However, during formation of radiative centers at the Si-nc/SiO_2 interfaces there are appearance of new broken bonds, which are the centers of nonradiative recombination. This is confirmed by the results of hydrogen passivation in these structures: the intensity of PL after passivating annealing in H_2 grows [76]. The destruction of photoluminescent centers at the annealing temperatures higher than 650 °C occurs due to the effusion of nitrogen from the film, which is confirmed by the profiles of nitrogen distribution after high-temperature annealing (Fig. 18a).

Melnik V.P., Popov V.G., Romanyuk B.M. et al. Luminescent properties of the structures with embedded silicon ...

295

Fig. 18. Distribution of nitrogen in the $SiO_{1.5}$ film after each stage of cyclic annealing: 1150 °C → 450 °C → 1150 °C (a) and X-ray photoelectron spectroscopy data after the first and second stages of annealing (b).

Thus, the mechanisms responsible for the PL intensity increasing after LT annealing in the mixture of oxygen and nitrogen are associated with the reconstruction of the Si-nc/SiO_2 interface and formation of the electron energy states involved in recombination of non-equilibrium charge carriers. Quasi-chemical reactions of these centers formation take place with participation of oxygen and nitrogen. The initial centers of these reactions are broken bonds at the Si-nc/SiO_2 interface.

7. Conclusions

The influence of the presence of the number of impurities (H, C, N, Al, Ti) on the processes of formation and modification of the luminescent properties inherent to the structures with silicon nanoclusters embedded into the dielectric matrix has been studied. It was ascertained that

the presence of carbon, nitrogen and aluminum in the high-temperature (1100…1200 °C) formation of Si-nc in the matrix of silicon dioxide significantly accelerates nucleation and growth of the silicon nanoclusters. The main mechanism of influence is the binding of excess oxygen in the growth region of Si-nc. Controlled implantation of impurities (at the level of 0.1 to 2 at.%) allows one to influence the size and concentration of nanoclusters and, accordingly, to change the spectral characteristics of the luminescent structures. In particular, the implantation of carbon and nitrogen increases the concentration of smaller clusters, which is accompanied by the increase (by several times) in the intensity of photoluminescence in the short-wave region of the spectrum. In addition, nitrogen effectively passivates the centers of non-radiative recombination, which leads to the overall increase in the intensity of radiative recombination. Aluminum, intensively absorbing oxygen, creates conditions for rapid formation of the Si-nc at the initial stages of their high-temperature formation.

It has been ascertained that the luminescent properties of the structures with Si-nc are influenced by the state of the nanocluster/matrix interface, and modification of this interface allows one to significantly increase the PL intensity. The presence at the interface of the transition layer with the thickness of several monolayers containing silicon suboxides leads to the increase in the PL intensity within the spectral range of 700 to 900 nm. The intensity of PL is proportional to the number of suboxide states and can be changed by implantation of impurities, temperature modification (annealing at $T \sim 450$ °C) and ultrasonic treatment. The mechanisms responsible for increasing the PL intensity are related to the reconstruction of the Si-nc/SiO_2 interface and formation of electron energy states involved in the recombination of non-equilibrium charge carriers. Quasi-chemical reactions to create these states occur with participation of oxygen and nitrogen, and the initial centers of reactions are the broken bonds at the interface Si-nc/SiO_2.

It has been shown that the combined use of the number of the technological procedures, namely: stimulated conditions for the formation of nanoclusters, modification of the Si-nc/SiO_2 interface, passivation of non-radiative recombination centers can significantly (up to 17 times) increase the efficiency of PL intensity as compared to traditional luminescent structures, namely, thermal decomposition of non-stoichiometric SiO_x film ($x \sim 1.5$).

Melnik V.P., Popov V.G., Romanyuk B.M. et al. Luminescent properties of the structures with embedded silicon ...

References

1. Canham L. Introductory lecture: origins and applications of efficient visible photoluminescence from silicon-based nanostructures. *Faraday Discuss*. 2020. **222**. P. 10–81. https://doi.org/10.1039/D0FD00018C.

2. Galář P., Popelář, T., Khun J. *et al*. The red and blue luminescence in silicon nanocrystals with oxidized, nitrogen-containing shell. *Faraday Discuss*. 2020. **222**. P. 1–12. https://doi.org/10.1039/C9FD00092E.

3. Tanaka K., Okamoto K. Photoluminescence spectroscopy of Si:SiO$_2$ films fabricated by radio frequency sputtering. *Key Eng. Mater*. 2018. **790**. P. 37–42. https://doi.org/10.4028/www.scientific.net/KEM.790.37.

4. Tuan N.T., Thu V.V., Trung D.Q. *et al*. On the origin of photoluminescence enhancement of Si nanocrystals on silica glass template and Si/SiO$_2$ superlattice. *Phys. B: Condens. Matter*. 2023. **662**, No 1. P. 414970. https://doi.org/10.1016/j.physb.2023.414970.

5. Yazicioglu D., Gutsch S., Zacharias M. Effects of field enhanced charge transfer on the luminescence properties of Si/SiO$_2$ superlattices. *Sci. Rep*. 2022. **12**, No 1. P. 2641. https://doi.org/10.1038/s41598-022-05566-4.

6. Michailovska K.V., Indutnyi I.Z., Shepeliavyi P.E. *et al*. Luminescent and Raman study of nanostructures formed upon annealing of SiO$_x$:Sm films. *SPQEO*. 2023. **26**, No 1. P. 068–075. https://doi.org/10.15407/spqeo26.01.068.

7. Wang X.X., Zhang J.G., Ding L. *et al*. Origin and evolution of photoluminescence from Si nanocrystals embedded in a SiO$_2$ matrix. *Phys. Rev. B*. 2005. **72**, No 19. P. 195313. https://doi.org/10.1103/PhysRevB.72.195313.

8. Mulloni V., Bellutti P., Vanzetti L. XPS and SIMS investigation on the role of nitrogen in Si nanocrystals formation. *Surf. Sci*. 2005. **585**, No 3. P. 137–143. https://doi.org/10.1016/j.susc.2005.03.059.

9. Comedi D.M., Zalloum O.H.Y., Irving E.A. *et al*. X-ray-diffraction study of crystalline Si nanocluster formation in annealed silicon-rich silicon oxides. *J. Appl. Phys*. 2006. **99**, No 2. P. 023518. https://doi.org/10.1063/1.2162989.

10. Pi X.D., Zalloum O.H.Y., Roschuk T. *et al*. Light emission from Si nanoclusters formed at low temperatures. *Appl. Phys. Lett*. 2006. **88**, No 10. P. 103111. https://doi.org/10.1063/1.2183813.

11. Boudreau M., Boumerzoug M., Mascher P., and Jessop P.E. Electron cyclotron resonance chemical vapor deposition of silicon oxynitrides using tris (dimethylamino) silane. *Appl. Phys. Lett*. 1993. **63.** P. 3014. https://doi.org/10.1063/1.110243.

12. Evtukh A., Bratus' O., Gorbanyuk T., Ievtukh V. Electrical characterization of SiO$_2$(Si) films as a medium for charge storage. *phys. status solidi (c)*. 2008. **5**, No 12. P. 3663–3666. https://doi.org/10.1002/pssc.200780165.

13. Lin G.-R., Lin C.-J. Lin C.-K. *et al*. Oxygen defect and Si nanocrystal dependent white-light and near-infrared electroluminescence of Si-implanted and plasma-enhanced chemical-vapor deposition-grown Si-rich SiO$_2$. *J. Appl. Phys*. 2005. **97**. P. 094306. https://doi.org/10.1063/1.1886274.

14. Sopinskyy M., Khomchenko V. Electroluminescence in SiO$_x$ films and SiO$_x$-film-based systems. *Cur. Opin. Solid State Mater. Sci*. 2003. **7**, No 2. P. 97–109. https://doi.org/10.1016/S1359-0286(03)00048-2.

15. Fronya A.A., Antonenko S.V., Derzhavin S.I. *et al*. Morphology and photoluminescence properties of silicon nanoparticles deposited in helium-nitrogen mixtures maintained at low residual pressures. *J. Phys.: Conf. Ser*. 2021. **2058**. P. 012011. https://doi.org/10.1088/1742-6596/2058/1/012011.

16. Tsoi E., Normand P., Nassiopoulou A.G. *et al*. Silicon nanocrystal memories by LPCVD of amorphous silicon, followed by solid phase crystallization and thermal oxidation. *J. Phys.: Conf. Ser*. 2005. **10**. P. 31–34. https://doi.org/10.1088/1742-6596/10/1/008.

17. Ioannou-Sougleridis V., Nassiopoulou A.G. Charging characteristics of Si nanocrystals embedded within SiO$_2$ in the presence of near-interface oxide traps. *J. Phys.: Conf. Ser*. 2005. **10**. P. 39–42. https://doi.org/10.1088/1742-6596/10/1/010.

18. Jambois O., Molinari M., Rinnert H., Vergnat M. Photoluminescence and electroluminescence of amorphous SiO$_x$ films prepared by reactive evaporation of silicon with oxygen. *Opt. Mater*. 2005. **27**, No 5. P. 107. https://doi.org/10.1016/j.optmat.2004.08.070.

19. Bratus' O.L., Evtukh A.A., Litvin O.S. *et al*. Structural properties of nanocomposite films SiO$_2$(Si) films obtained by ion-plasma sputtering and thermal annealing. *SPQEO*. 2011. **14**, No 2. P. 247–255. https://doi.org/10.15407/spqeo14.02.247.

20. Bratus O.L., Evtukh A.A., Ilchenko V.V. Peculiarities of electron transport in SiO$_x$ films obtained by ion-plasma sputtering. *Appl. Nanosci*. 2020. **10**. P. 2723–2729. https://doi.org/10.1007/s13204-019-00988-5.

21. Fronya A.A., Antonenko S.V., Kharin A.Yu. *et al*. Tailoring photoluminescence from Si-based nanocrystals prepared by pulsed laser ablation in He-N$_2$ gas mixtures. *Molecules*. 2020. **25**, No 3. P. 440. https://doi.org/10.3390/molecules25030440.

22. Kahler U. Darstellung, Charakterisierung und Oberflächenmodifizierung von Siliziumnanopartikeln in SiO$_2$: *Dissertation des Dr.-Ing., Mathematisch-Naturwissenschaftlich-Technischen Fakultät der Martin-Luther-Universität Halle-Wittenberg*. 2001. http://dx.doi.org/10.25673/2920.

23. Dan'ko V.A., Bratus' V.Ya, Indutnyi I.Z. *et al*. Controlling the photoluminescence spectra of porous nc-Si–SiO$_x$ structures by vapor treatment. *SPQEO*. 2010. **13**, No 4. P. 413–417. https://doi.org/10.15407/spqeo13.04.413.

24. Meldrum A., Hryciw A., Buchanan K.S. *et al*. Two-dimensionally-patterned silicon nanocrystal arrays. *Opt. Mater*. 2005. **27**, No 5. P. 812–817. https://doi.org/10.1016/j.optmat.2004.08.003.

Melnik V.P., Popov V.G., Romanyuk B.M. et al. Luminescent properties of the structures with embedded silicon …

297

25. Barba D., Martin F., Dahmoune C., Ross G.G. Effects of oxide layer thickness on Si-nanocrystal photoluminescence intensity in Si$^+$-implanted SiO$_2$/Si systems. *Appl. Phys. Lett.* 2006. **89**, No 3. P. 034107. https://doi.org/10.1063/1.2234739.

26. Normand P., Kapetanakis E., Dimitrakis P. *et al.* Nanocrystals manufacturing by ultra-low-energy ion-beam-synthesis for non-volatile memory applications. *Nucl. Instrum. Meth. B*. 2004. **216**. P. 228. https://doi.org/10.1016/j.nimb.2003.11.039.

27. Kapetanakis E., Normand P., Tsoukalas D. *et al.* Charge storage and interface states effects in Si-nanocrystal memory obtained using low-energy Si implantation and annealing, *Appl. Phys. Lett*. 2000. **77**, No 21. P. 3450–3452. https://doi.org/10.1063/1.1328101.

28. González-Varona O., Garrido B., Pérez-Rodríguez A. *et al*. Charge storage effects in Si nanocrystals embedded in SiO$_2$ thin films. *Solid State Phenom.* 2001. **80–81**. P. 243. https://doi.org/10.4028/www.scientific.net/SSP.80-81.243.

29. Mizuno T., Kanazawa R., Aoki T., Sameshima T. SiC quantum dot formation in SiO$_2$ layer using double hot-Si$^+$/C$^+$-ion implantation technique. *Jpn. J. Appl. Phys.* 2020. **59**. SGGH02. https://doi.org/10.7567/1347-4065/ab5bc4.

30. Pelletier J., Anders A. Plasma-based ion implantation and deposition: a review of physics, technology, and applications. *IEEE Trans. Plasma Sci.* 2005. **33**, No 6. P. 1944–1959. https://doi.org/10.1109/TPS.2005.860079.

31. Dan'ko V.A., Indutnyi I.Z., Lysenko V.S. *et al.* Kinetics of structural and phase transformations in thin SiO$_x$ films in the course of a rapid thermal annealing. *Semiconductors.* 2005. **39**, No 10. P. 1197. https://doi.org/10.1134/1.2085270.

32. Sarikov A., Litovchenko V., Lisovskyy I. *et al.* Role of oxygen migration in the kinetics of the phase separation of nonstoichiometric silicon oxide films during high-temperature annealing. *Appl. Phys. Lett.* 2007. **91**, No 13. P. 133109. https://doi.org/10.1063/1.2790814.

33. Daldosso N., Das G., Larcheri S. *et al.* Silicon nanocrystal formation in annealed silicon-rich silicon oxide films prepared by plasma enhanced chemical vapor deposition. *J. Appl. Phys.* 2007. **101**, No 11. P. 113510. https://doi.org/10.1063/1.2740335.

34. Lioudakis E., Othonos A., Hadjisavvas G.C. *et al.* Quantum confinement and interface structure of Si nanocrystals of sizes 3–5 nm embedded in a-SiO$_2$. *Physica E: Low Dimens. Syst. Nanostruct.* 2007. **38**, No 1–2. P. 128–134. https://doi.org/10.1016/j.physe.2006.12.020.

35. Luppi M., Ossicini S. *Ab initio* study on oxidized silicon clusters and silicon nanocrystals embedded in SiO$_2$: Beyond the quantum confinement effect. *Phys. Rev. B.* 2005. **71**, No 3. P. 035340. https://doi.org/10.1103/PhysRevB.71.035340.

36. Hadjisavvas G., Remediakis I.N., Kelires P. Shape and faceting of Si nanocrystals embedded in a-SiO$_2$: A Monte Carlo study. *Phys. Rev. B.* 2006. **74**, No 16. P. 165419. https://doi.org/10.1103/PhysRevB.74.165419.

37. Garrido B., López M., Pérez-Rodríguez A. *et al.* Optical and electrical properties of Si-nanocrystals ion beam synthesized in SiO$_2$. *Nucl. Instrum. Methods Phys. Res. B.* 2004. **216.** P. 213–221. https://doi.org/10.1016/j.nimb.2003.11.037.

38. Kang X., Zhu M. Tailoring the photoluminescence of atomically precise nanoclusters. *Chem. Soc. Rev.* 2019. **48**. P. 2422–2457. https://doi.org/10.1039/C8CS00800K.

39. Nélis A., Haye E., Terwagne G. Influence of oxygen co-implantation on germanium out-diffusion and nanoclustering in SiO$_2$/Si films. *Thin Solid Films.* 2022. **746**, No 21. P. 139135. https://doi.org/10.1016/j.tsf.2022.139135.

40. Mizuno T., Yamamoto M., Nakada S. *et al.* SiC nano-dot formation in bulk-Si substrate using hot-C$^+$-ion implantation process. *Jpn. J. Appl. Phys.* 2019. **58**. P. 081004. https://doi.org/10.7567/1347-4065/ab2ac9.

41. Yu D., Lee S., Hwang G.S. On the origin of Si nanocluster formation in a Si suboxide matrix. *J. Appl. Phys.* 2007. **102**, No 8. P. 084309. https://doi.org/10.1063/1.2800268.

42. Burdov V.A. Dependence of the optical gap of Si quantum dots on the dot size. *Semiconductors.* 2002. **36**, No 10. P. 1233–1236. https://doi.org/10.1134/1.1513861.

43. Evtukh A., Hartnagel H., Yilmazoglu O., Mimura H., Pavlidis D. *Vacuum Nanoelectronic Devices. Novel Electron Sources and Applications*. John Willey & Son Ltd, 2015.

44. Conibeer G., Green M., Cho E.-C. *et al.* Silicon quantum dot nanostructures for tandem photovoltaic cells. *Thin Solid Films.* 2008. **516**, No 20. P. 6748–6756. https://doi.org/10.1016/j.tsf.2007.12.096.

45. Rebohle L., von Borany J., Yankov R.A. *et al.* Strong blu and violet photo- and electroluminescence from germanium-implanted and silicon-implanted silicon dioxide layers. *Appl. Phys. Lett.* 1997. **71**, No 19. P. 2809–2811. https://doi.org/10.1063/1.120143.

46. Tyschenko I.E., Rebohle L., Yankov R.A. Enhancement of the intensity of the short-wave-length visible photoluminescence from silicon-implanted silicon dioxide films caused by hydrostatic pressure during annealing. *Appl. Phys. Lett.* 1998. **73**, No 10. P. 1418–1420. https://doi.org/10.1063/1.121962.

47. Yi L.X., Heitmann J., Scholtz R. *et al.* Si rings, Si clusters, and Si nanocrystals – different states of ultrathin SiO$_x$ layers. *Appl. Phys. Lett.* 2002. **81**, No 22. P. 661–663. https://doi.org/10.1063/1.1525051.

48. Kanzawa Y., Kageyama T., Takeoka S. *et al.* Size-dependent near-infrared photoluminescence spectra of Si nanocrystals embedded in SiO$_2$ matrices. *Solid State Commun.* 1997. **102**, No 7. P. 533–537. https://doi.org/10.1016/S0038-1098(96)00774-0.

Melnik V.P., Popov V.G., Romanyuk B.M. et al. Luminescent properties of the structures with embedded silicon ...

298

49. Gavrilchenko I.V., Milovanov Y.S., Gryn S.V. *et al.* Spectral-luminescence properties of freestanding porous SiC layers. *J. Lumin.* 2021. **240**, No 1. P. 118466. https://doi.org/10.1016/j.jlumin.2021.118466.

50. Inokuma T., Wakayama Y., Muramoto T. *et al.* Optical properties of Si clusters and Si nanocrystallites in high-temperature annealed SiO$_x$ films. *J. Appl. Phys.* 1998. **83**, No 4. P. 2228–2234. https://doi.org/10.1063/1.366961.

51. Rinnert H., Vergnat M., Burneau A. Evidence of light-emitting amorphous silicon clusters confined in a silicon oxide matrix. *J. Appl. Phys.* 2001. **89**, No 1. P. 237–243. https://doi.org/10.1063/1.1330557.

52. Zatsepin A., Biryukov D. Temperature effects in the photoluminescence of semiconductor quantum dots, in: *Quantum Dots. Fundamental and Applications.* Ed. F. Divsar. London, IntechOpen, 2020.

53. Irrera A., Pacifici D., Miritello M., Franzo G. Excitation and de-excitation properties of silicon quantum dots under electrical pumping. *Appl. Phys. Lett.* 2002. **81**, No 10. P. 1866–1868. https://doi.org/10.1063/1.1505117.

54. Hryciw A., Meldrum A., Buchanan K.S., White C.W. Effects of particle size and excitation spectrum on the photoluminescence of silicon nanocrystals formed by ion implantation. *Nucl. Instrum. Methods Phys. Res. B.* 2004. **222**, No 3–4. P. 469–476. https://doi.org/10.1016/j.nimb.2004.02.025.

55. Shimizu-Iwayama T., Kurumado N., Hole D.E., Townsend P.D. Optical properties of silicon nanoclusters fabricated by ion implantation. *J. Appl. Phys.* 1998. **83**, No 11. P. 6018–6022. https://doi.org/10.1063/1.367469.

56. Cheylan S., Elliman R.G. The effect of ion dose and annealing ambient on room temperature photoluminescence from Si nanocrystals in SiO$_2$. *Nucl. Instrum. Methods Phys. Res. B.* 1999. **148**, No 1–4. P. 986–990. https://doi.org/10.1016/S0168-583X(98)00771-X.

57. Sias U.S., Amaral L., Behar M. *et al.* Photo-luminescence behavior of Si nanocrystals as a function of the implantation temperature and excitation power density. *J. Appl. Phys.* 2005. **98**, No 3. P. 034312. https://doi.org/10.1063/1.1989437.

58. Sias U.S., Behar M., Boudinov H., Moreira E.C. Influence of the implantation and annealing parameters on the photoluminescence produced by Si hot implantation. *Nucl. Instrum. Methods Phys. Res. B.* 2007. **257**, No 1–2. P. 51–55. https://doi.org/10.1016/j.nimb.2006.12.114.

59. Fernandez B.G., López M., García C. *et al.* Influence of average size and interface passivation on the spectral emission of Si nanocrystals embedded in SiO$_2$. *J. Appl. Phys.* 2002. **91**, No 2. P. 798–807. https://doi.org/10.1063/1.1423768.

60. Lisovskyy I., Voitovych M., Litovchenko V. *et al.* Radiation induced enhancement of hydrogen influence on luminescent properties of nc-Si/SiO$_2$ structures. *Nanoscale Res. Lett.* 2016. **11**, No 1. P. 545. https://doi.org/10.1186/s11671-016-1744-7.

61. Wu X., Bek A., Bittner A.M. *et al.* The effect of annealing conditions on the red photoluminescence of nanocrystalline Si/SiO$_2$ films. *Thin Solid Films.* 2003. **425**, No 1–2. P. 175–184. https://doi.org/10.1016/S0040-6090(02)01113-6.

62. Wilkinson A.R., Elliman R.G. Kinetics of H$_2$ passivation of Si nanocrystals in SiO$_2$. *Phys. Rev. B.* 2003. **68**, No 15. P. 155302. https://doi.org/10.1103/PhysRevB.68.155302.

63. Tetelbaum D.I., Trushin S.A., Burdov V.A. *et al.* The influence of phosphorus and hydrogen ion implantation on the photoluminescence of SiO$_2$ with Si nanoinclusions. *Nucl. Instrum. Methods Phys. Res. B.* 2001. **174**, No 1–2. P. 123–129. https://doi.org/10.1016/S0168-583X(00)00457-2.

64. Dalba G., Daldosso N., Fornasini P. *et al.* Chemical composition and local structure of plasma enhanced chemical vapor-deposited Si nanodots and their embedding silica matrix. *Appl. Phys. Lett.* 2003. **82**, No 6. P. 889–891. https://doi.org/10.1063/1.1543641.

65. Bi L., He Y., Feng J.Y. Effect of post-annealing in oxygen atmosphere on the photoluminescence properties of nc-Si rich SiO$_2$ films. *J. Cryst. Growth.* 2006. **289**, No 2. P. 564–567. https://doi.org/10.1016/j.jcrysgro.2005.12.014.

66. Caristia L., Nicotra G., Bongiorno C. *et al.* The influence of hydrogen and nitrogen on the formation of Si nanoclusters embedded in sub-stoichiometric silicon oxide layers. *Microelectron. Reliab.* 2007. **47**, No 4–5. P. 777–780. https://doi.org/10.1016/j.microrel.2007.01.056.

67. Kachurin G.A., Yanovskaya S.G., Zhuravlev K.S. *et al.* The role of nitrogen in the formation of luminescent silicon nanoprecipitates upon annealing of SiO$_2$ layers implanted with Si ions. *Semiconductors.* 2001. **35**, No 10. P. 1182–1186. https://doi.org/10.1134/1.1410661.

68. Tetelbaum D.I., Mikhaylov A.N., Vasiliev V.K. *et al.* Effect of carbon implantation on visible lumines-cence and composition of Si-implanted SiO$_2$ layers. *Surf. Coat. Technol.* 2009. **203**, No 17–18. P. 2658–2663. https://doi.org/10.1016/j.surfcoat.2009.02.087.

69. Zhuge L.J., Wu X.M., Li Q. *et al.* Origin of violet photoluminescence in SiO$_2$ films co-doped with silicon and carbon. *Physica E: Low Dimens. Syst. Nanostruct.* 2004. **23**, No 1–2. P. 86–91. https://doi.org/10.1016/j.physe.2004.01.002.

70. Ishikawa Y., Vasin A.V., Salonen J. *et al.* Color control of white photoluminescence from carbon-incorporated silicon oxide. *J. Appl. Phys.* 2008. **104**, No 8. P. 083522. https://doi.org/10.1063/1.3003079.

71. Ran G.Z., Wang S.T., Fu J.S. *et al.* Enhancing elec-troluminescence from Au/nanoscale Si-rich SiO$_2$ film/*p*-Si by doping Al into the SiO$_2$ film and γ-ray irradiation. *J. Lumin.* 2001. **93**, No 1. P. 75–80. https://doi.org/10.1016/S0022-2313(01)00164-8.

Melnik V.P., Popov V.G., Romanyuk B.M. et al. Luminescent properties of the structures with embedded silicon …

299

72. Wang Y.Q., Smirani R., Ross G.G. Effect of hydrogen passivation on the microstructure of silicon nanocrystals in SiO₂. *Physica E: Low Dimens. Syst. Nanostruct.* 2004. **23**, No 1–2. P. 97–101. https://doi.org/10.1016/j.physe.2004.01.001.

73. Dal Negro L., Yi J.H., Michel J. *et al.* Light emission efficiency and dynamics in silicon-rich silicon nitride films. *Appl. Phys. Lett.* 2006. **88**, No 23. P. 233109. https://doi.org/10.1063/1.2208378.

74. Iwayama T.S., Hama T., Hole D.E. Lamp annealing effects on the formation process of implanted silicon nanocrystals in SiO₂. *Nucl. Instrum. Methods Phys. Res. B.* 2007. **257**, No 1–2. P. 85–89. https://doi.org/10.1016/j.nimb.2006.12.166.

75. Romanyuk B.N., Melnik V.P., Popov V.G. *et al.* Effect of high-temperature annealing on photoluminescence of silicon nanocluster structures. *Semiconductors.* 2010. **44**, No 4. P. 514–518. https://doi.org/10.1134/S1063782610040184.

76. Khatsevych I., Melnik V., Popov V. *et al.* Effect of low-temperature treatments on photoluminescence enhancement of ion-beam synthesized Si nanocrystals in SiO₂ matrix. *SPQEO.* 2008. **11**, No 4. P. 352–355. https://doi.org/10.15407/spqeo11.04.352.

77. Romanyuk A., Melnik V., Olikh Y. *et al.* Light emission from nanocrystalline silicon clusters embedded in silicon dioxide: Role of the suboxide states. *J. Lumin.* 2010. **130**, No 1. P. 87–91. https://doi.org/10.1016/j.jlumin.2009.07.021.

78. Romanyuk B., Krüger D., Melnik V. *et al.* Ultrasound effect on radiation damages in boron implanted silicon. *SPQEO.* 2000. **3**, No 1. P. 15–18. https://doi.org/10.15407/spqeo3.01.015.

79. Romanyuk B., Melnik V., Olikh Ya. *et al.* Modification of the Si amorphization process by *in-situ* ultrasonic treatments during ion implantation. *Semicond. Sci. Technol.* 2001. **16**. P. 397. https://doi.org/10.1088/0268-1242/16/5/320.

80. Sassella A., Borghesi A., Corni F. *et al.* Infrared study of Si-rich silicon oxide films deposited by plasma-enhanced chemical vapor deposition. *J. Vac. Sci. Technol. A.* 1997. **15**, No 2. P. 377–389. https://doi.org/10.1116/1.580495.

81. Müller T., Heinig K.-H., Möller W. Size and location control of Si nanocrystals at ion beam synthesis in thin SiO₂ films. *Appl. Phys. Lett.* 2002. **81**. P. 3049–3051. https://doi.org/10.1063/1.1512952.

82. Nicotra G., Spinella C., La Magna A. *et al.* Quantitative study of the Si/SiO₂ phase separation in substoichiometric silicon oxide films. *Mater. Sci. Eng. B.* 2009. **159–160**. P. 80–82. https://doi.org/10.1016/j.mseb.2008.10.045.

83. Rochet F., Dufour G., Roulet H. *et al.* Modification of SiO through room-temperature plasma treatments, rapid thermal annealing, and laser irradiation in a non-oxidizing atmosphere. *Phys. Rev. B.* 1988. **37**, No 11. P. 6468. https://doi.org/10.1103/PhysRevB.37.6468.

84. Lisovskyy I.P., Voitovich M.V., Sarikov A.V. *et al.* Transformation of the structure of silicon oxide during the formation of Si nanoinclusions under thermal annealings. *Ukr. J. Phys.* 2009. **54**, No 4. P. 383–390.

85. Lisovsky I.P., Litovchenko V.G., Voitovych M.V. *et al.* Influence of γ-irradiation on optical properties of nitrogen-doped nc-Si/SiO₂ structures. *Ukr. J. Phys.* 2008. **53**, No 10. P. 997–1001.

86. Zacharias M., Heitmann J., Scholz R. *et al.* Size-controlled highly luminescent silicon nanocrystals: A SiO/SiO₂ superlattice approach. *Appl. Phys. Lett.* 2002. **80**, No 4. P. 661–663. https://doi.org/10.1063/1.1433906.

87. Delerue C., Allan G., Lannoo M. Optical band gap of Si nanoclusters. *J. Lumin.* 1998. **80**, No 1–4. P. 65–73. https://doi.org/10.1016/S0022-2313(98)00071-4.

88. Yang M.-S., Cho K.-S., Jhe J.-H. *et al.* Effect of nitride passivation on the visible photoluminescence from Si-nanocrystals. *Appl. Phys. Lett.* 2004. **85**, No 16. P. 3408–3410. https://doi.org/10.1063/1.1787599.

89. Ternon C., Gourbilleau F., Dufour C. *et al.* Room temperature visible light emission from Si/SiO₂ multilayers: Roles of interface electronic states and silicon phase. *J. Lumin.* 2002. **99**, No 4. P. 361–364. https://doi.org/10.1016/S0022-2313(02)00374-5.

90. De La Torre J., Bremond G., Souifi A. *et al.* Simultaneous observation of 'Self Trapped Exciton' and Q-confined exciton luminescence emission in silicon nanocrystals. *Opt. Mater.* 2005. **27**, No 5. P. 1004–1007. https://doi.org/10.1016/j.optmat.2004.08.053.

91. Murarca S. *Silicides for VLSI Applications.* Academic, New York. 1983.

92. Chase M.W. NIST-JANAF Themochemical Tables, Fourth Edition. *J. Phys. Chem. Ref. Data, Monograph.* 1998. **9**. P. 1–1951.

93. Zumdahl S.S. *Chemical Principles. 8th Ed.* Houghton Mifflin Company, 2015.

94. Assali L.V.C., Machado W.V.M., Justo J.F. Titanium impurities in silicon, diamond, and silicon carbide. *Braz. J. Phys.* 2004. **34**, No 2b. P. 602–604. https://doi.org/10.1590/S0103-97332004000400016.

95. Rohatgi A., Davis J.R., Hopkins R.H., McMullin P.G. A study of grown-in impurities in silicon by deep-level transient spectroscopy. *Solid-State Electronics.* 1983. **26**, No 11. P. 1039–1051. https://doi.org/10.1016/0038-1101(83)90001-1.

96. Kaganovich E.B., Lisovsky I.P., Manoilov E.G., Zlobin S.A. Photoluminescence of nanocrystalline silicon films obtained by pulsed laser deposition with carbon introduction. *Semiconductors.* 2006. **40**. P. 443–448. https://doi.org/10.1134/S1063782606040130.

97. Kanemitsu Y., Suzuki K., Kyushin S., Matsumoto H. Visible photoluminescence from silicon-back-bone polymers. *Phys. Rev. B.* 1995. **51**, No 19. P. 13103–13110. https://doi.org/10.1103/PhysRevB.51.13103.

Melnik V.P., Popov V.G., Romanyuk B.M. et al. Luminescent properties of the structures with embedded silicon ...

300

98. Kanemitsu Y., Ogawa T., Shiraishi K., Takeda K. Visible photoluminescence from oxidized Si nanometer-sized spheres: Exciton confinement on a spherical shell. *Phys. Rev. B.* 1993. **48**, No 7. P. 4883–4886. https://doi.org/10.1103/PhysRevB.48.4883.

99. Matsumoto T., Takahashi J., Tamaki T. *et al.* Blue-green luminescence from porous silicon carbide. *Appl. Phys. Lett.* 1994. **64**, No 2. P. 226–228. https://doi.org/10.1063/1.111979.

100. Lindhard J., Scharff M. Energy dissipation by ions in the kev region. *Phys. Rev.* 1961. **124**, No 1. P. 128–130. https://doi.org/10.1103/PhysRev.124.128.

101. Oberemok O., Litovchenko V., Popov V. *et al.* Formation of silicon nanoclusters in buried ultra-thin oxide layers. *SPQEO.* 2011. **14**, No 3. P. 269–272. https://doi.org/10.15407/spqeo14.03.269.

102. Litovchenko V., Romanyuk B., Melnik V. *et al.* Stimulated creation of the SOI structures with Si nanoclusters by low-dose SIMOX technology. *Solid State Phenom.* 2011. **178**–**179**. P. 17–24. https://doi.org/10.4028/www.scientific.net/SSP.178-179.17.

103. Gamov D., Khatsevych I., Lytovchenko V. *et al.* Influence of nitrogen impurity on photoluminescence of silicon nanoclusters in SiO$_2$ matrix. *Ukr. J. Phys.* 2009. **54**, No 4. P. 413–417.

104. Fahey P.M., Griffin P.B., Plummer J.D. Point defects and dopant diffusion in silicon. *Rev. Mod. Phys.* 1989. **61**, No 2. P. 289–384. https://doi.org/10.1103/RevModPhys.61.289.

105. Lisovski I.P., Litovchenko V.G., Lozinski V.B. *et al.* Structural and electrical properties of ultrathin SiO$_2$ film on silicon. *Proc. 3rd Int. Symposium "The Physics and Chemistry of SiO$_2$ and the Si-SiO$_2$ Interface".* The Electrochem. Soc. Inc., Pennington, NJ, USA. 1996. **3**. P. 592–603.

106. Wilkinson A.R., Elliman R.G. The effect of annealing environment on the luminescence of silicon nano-crystals in silica. *J. Appl. Phys.* 2004. **96**, No 7. P. 4018–4020. https://doi.org/10.1063/1.1789265.

107. Baran M., Bulakh B., Korsunska N. *et al.* Role of silicon oxide defects in emission process of Si-SiO$_2$ systems. *SPQEO.* 2003. **6**, No 3. P. 282–286. https://doi.org/10.15407/spqeo06.03.282.

Authors and CV

Viktor Melnik, Professor, acting director of the ISP NAS of Ukraine, was born in 1963. He defended Dr. of Sci. thesis in 2012 (Physics and Mathematics) at the V. Lashkaryov Institute of Semiconductor Physics, NAS of Ukraine. Author of more than 250 scientific publications. His main research activity is in the fields of ion-beam engineering and diagnostics.
E-mail: vp_mel@ukr.net,
https://orcid.org/0000-0002-8670-7415

Valentin Popov was born in 1946. He defended PhD thesis in 1980 (Physics and Mathematics) at the V. Lashkaryov Institute of Semiconductor Physics, NAS of Ukraine. He is Senior Researcher in the Department of Ion Beam Engineering and Structure Analysis at the same institute. Authored more than 260 scientific publications. His main research activity is in the fields of layered structures with nanoclusters subjected to ion-beam modification.
E-mail: romb@isp.kiev.ua,
http//orcid.org/0000-0002-9992-9770

Boris Romanyuk was born in 1946. He defended DrSc thesis in 1980 (Physics and Mathematics) at the V. Lashkaryov Institute of Semiconductor Physics, NAS of Ukraine. Head of the Department of Ion Beam Engineering and Structural Analysis at the same institute. Professor B. Romanyuk has authored more than 270 scientific publications. His research interests include: physics of semiconductors and dielectrics, ion-beam engineering and conducting a wide range of studies of semiconductor structures.
E-mail: romb@isp.kiev.ua,
https://orcid.org/0000-0002-1688-7588

Serhii Antonin was born in 1994, defended his PhD thesis in applied physics and nanomaterials in 2022. Junior researcher at the V. Lashkaryov Institute of Semiconductor Physics, NAS of Ukraine. The area of his scientific interests includes nanomaterials and nanostructures, composite films, semiconductor technologies and solar cells. https://orcid.org/0000-0003-1607-9721

Anatoliy Evtukh was born in 1955, he defended his PhD thesis in Physics and Mathematics (Physics of Semiconductors and Dielectrics) in 1985 and Dr. of Sci. thesis in 2004 at the V. Lashkaryov Institute of Semiconductor Physics, NASU. Leading Researcher of the Department of Physics of Surface and Nanophotonics at the same institute. Prof. A. Evtukh has authored over 300 publications. His main research activity is in the field of nanomaterials and nanostructures, composite films with semiconductor and metal nanoinclusions, electron transport, surface physics, semiconductor technologies, sensors and solar cells.
E-mail: anatoliy.evtukh@gmail.com,
https://orcid.org/0000-0003-3527-9585

Melnik V.P., Popov V.G., Romanyuk B.M. et al. Luminescent properties of the structures with embedded silicon ...

301

Authors' contributions

Melnik V.P.: key ideas, investigations, conceptualization.
Popov V.G.: investigations, initial draft preparation, discussion.
Romanyuk B.M.: conceptualization, key ideas, validation, supervision.
Antonin S.V.: initial draft preparation, writing.
Evtukh A.A.: conceptualization, writing – review & editing, analysis, validation.

Люмінесцентні властивості структур із вбудованими кремнієвими нанокластерами: вплив технології, легування та відпалу (Огляд)

В.П. Мельник, В.Г. Попов , Б.М. Романюк, С.В. Антонін, А.А. Євтух

Анотація. Виявлення фотолюмінесценції (ФЛ) у традиційно нелюмінесцентному матеріалі Si (типово непрямозонного напівпровідника) привертає велику увагу як у науковому аспекті, так і для застосувань у сферах мікро- та наноелектроніки і фотоелектроніки. Незважаючи на успіх у технології та розумінні багатьох особливостей характеристик ФЛ, багато проблем ще не вирішено. Зокрема, які механізми походження ліній ФЛ – квантово-розмірні, молекулярні комплекси всередині SiO_2, інтерфейсні або об'ємні локалізовані стани і т. ін. Як досягти збільшення інтенсивності ФЛ та створення ФЛ у різних ділянках спектра. Запропонований огляд систематизує результати, пов'язані з такими проблемами, з використанням оригінальних технологій створення Si-нанокристалів (Si-нк) та різних методів досліджень. На закінчення, ми підсумовуємо результати щодо властивостей люмінесцентних структур Si-нк–SiO_2 в залежності від технології синтезу, фото- та структурних властивостей і перспектив застосування для мікро- та наноелектроніки і фотоелектроніки.

Ключові слова: кремній, нанокластер, фотолюмінесценція, іонно-променевий синтез, легування, відпал.

Melnik V.P., Popov V.G., Romanyuk B.M. et al. Luminescent properties of the structures with embedded silicon ...

302